A Complex Magma Mixing Origin for Rocks Erupted in 1915, Lassen Peak, California

MICHAEL A. CLYNNE*

US GEOLOGICAL SURVEY, 345 MIDDLEFIELD ROAD MS910, MENLO PARK, CA 94025, USA

The eruption of Lassen Peak in May 1915 produced four volcanic rock types within 3 days, and in the following order: (1) hybrid black dacite lava containing (2) undercooled andesitic inclusions, (3) compositionally banded pumice with dark andesite and light dacite bands, and (4) unbanded light dacite. All types represent stages of a complex mixing process between basaltic andesite and dacite that was interrupted by the eruption. They contain disequilibrium phenocryst assemblages characterized by the co-existence of magnesian olivine and quartz and by reacted and unreacted phenocrysts derived from the dacite. The petrography and crystal chemistry of the phenocrysts and the variation in rock compositions indicate that basaltic andesite intruded dacite magma and partially hybridized with it. Phenocrysts from the dacite magma were reacted. Cooling, crystallization, and vesiculation of the hybrid andesite magma converted it to a layer of mafic foam. The decreased density of the andesite magma destabilized and disrupted the foam. Blobs of foam rose into and were further cooled by the overlying dacite magma, forming the andesitic inclusions. Disaggregation of andesitic inclusions in the host dacite produced the black dacite and light dacite magmas. Formation of foam was a dynamic process. Removal of foam propagated the foam layer downward into the hybrid andesite magma. Eventually the thermal and compositional contrasts between the hybrid andesite and black dacite magmas were reduced. Then, they mixed directly, forming the dark andesite magma. About 40–50% andesitic inclusions were disaggregated into the host dacite to produce the hybrid black dacite. Thus, disaggregation of inclusions into small fragments and individual crystals can be an efficient magma-mixing process. Disaggregation of undercooled inclusions carrying reacted host-magma phenocrysts produces co-existing reacted and unreacted phenocryst populations.

KEY WORDS: *magma mixing; undercooled inclusions; disequilibrium phenocryst populations; banded pumice; Lassen*

INTRODUCTION

Magma mixing is an important process among intermediate magmas in volcanic arcs (e.g. Turner & Campbell, 1986; Philpotts, 1990, and references therein). Laboratory studies of synthetic analogs of silicate magma systems and mathematical modeling of mixing viscous liquids have suggested a range of possible mixing mechanisms (e.g. Cashman & Bergantz, 1991). However, use of these results to interpret magmatic systems is limited by the applicability of synthetic analogs to magmatic conditions and by the imprecise knowledge of the effective viscosity of silicate liquid–crystal mixtures at magmatic temperatures and pressures. If magmas mix incompletely, i.e. mingle, features such as compositional banding or undercooled inclusions are usually apparent, but if they mix completely, mineralogical disequilibrium may be the only direct evidence for a mixing origin.

If the thermal and compositional contrasts between two magmas are great and the ratio of silicic to mafic magma is large, there is little interaction between them, and the mafic magma is undercooled (e.g. Bacon, 1986). Many undercooled inclusions contain reacted phenocrysts inherited from their host silicic magma (Heiken & Eichelberger, 1980), and Bacon (1986) pointed out that undercooled inclusions are typically formed from hybrid magmas. In general, the formation of undercooled inclusions retards further mixing (Sakuyama, 1984; Thompson & Dungan, 1985; Sparks & Marshall, 1986; Koyaguchi & Blake, 1991). However, fragmentation and/or disaggregation of undercooled inclusions plays an important role in hybridization in some magma systems (Thompson & Dungan, 1985; Coulon et al., 1986; Clynne & Christiansen, 1987; Clynne, 1989; Linneman & Myers, 1990; Feeley & Dungan, 1996).

*Telephone: 650 329-5236. e-mail: mclynne@mojave.wr.usgs.gov

The products of the 1915 eruptions of Lassen Peak show abundant evidence of significant interaction between host and inclusion-forming magmas before undercooled inclusions formed. Moreover, further mixing occurred by the disaggregation of undercooled inclusions to produce homogeneous-appearing hybrid lava. Phenocrysts from the host dacite reacted with mafic magma, froze into inclusions, and were subsequently recycled back into their host to produce coexisting populations of reacted and unreacted phenocrysts. This paper integrates the physical and compositional details preserved in crystals with geochemical and volcanologic information, to explain the magma-mixing processes that produced the rock types erupted at Lassen Peak in 1915.

GEOLOGIC CONTEXT

The volcanic rocks of the southernmost Cascade Range are predominantly basaltic to andesitic that were erupted from small, short-lived volcanoes. However, a few long-lived, much larger volcanic centers have each erupted first andesite, then silicic andesite, and finally, dacite–rhyolite (Clynne, 1990). At the Lassen volcanic center (LVC), the Brokeoff Volcano, an 80 km³ andesitic stratocone formed between 0·60 and 0·40 Ma. Two episodes of silicic volcanism produced a dacite domefield totaling 30–50 km³. Between 0·3 and 0·2 Ma, two-pyroxene–hornblende dacite domes were erupted, and since 0·1 Ma hornblende–biotite dacite erupted as domes, lava flows and pyroclastic flows. Also, since 0·3 Ma, about 10 km³ of hybrid andesite consisting of thoroughly mixed mafic and silicic magma has intermittently erupted from the margins of the dacite domefield. The hybrid andesites and ubiquitous undercooled inclusions in dacites at LVC are evidence for interaction of regional basaltic to andesitic magma with silicic magma.

Lassen Peak, the site of the 1915 eruption, is itself a large (~2 km³), 28·3 ka, dacite dome that contains a disequilibrium phenocryst assemblage, abundant andesitic inclusions, and evidence of disaggregation of those inclusions (Turrin *et al.*, 1998).

THE 1915 ERUPTION

The stratigraphy of the May 1915 eruption (Christiansen & Clynne, 1986; in preparation) constrains the timing of mixing events and physical relations of magma types erupted. In mid-May 1915, after a year of intermittent steam blasts and formation of a summit crater of 350 m width, lava welled into the crater and formed a small dome of black glassy dacite. On the night of May 19, the growing dome was disrupted by a large phreatic explosion. Fragments of the still-hot dome fell on the snow-covered upper flanks of the northeastern side of Lassen Peak, which generated an avalanche that flowed down a path of 0·8 km width × 5 km length. Fragmentation of the avalanching lava blocks melted enough snow to generate a large debris flow. Dacite lava erupted from the vent unplugged by the explosion, spilled over the crater rims, and flowed ~300 m downslope.

After two quiet days, an explosive subplinian eruption on the afternoon of May 22 produced a new crater and erupted compositionally banded dacite and andesite pumice, followed by unbanded dacite pumice. Fallback of pumice generated a pyroclastic flow that swept across and incorporated snow from the still partly snow-covered northeast slope of Lassen Peak. By the time it reached the lower slope of the northeast flank of Lassen Peak, melting of the incorporated snow transformed the pyroclastic flow into a highly fluid debris flow. Continued pumice fall deposited a fallout lobe traceable for 25 km to the east and produced several smaller viscous debris flows on the flanks of Lassen Peak.

ANALYTICAL TECHNIQUES

Mineral analyses were obtained with an automated nine-spectrometer ARL SEMQ electron microprobe in Menlo Park using wavelength-dispersive analysis and the matrix correction procedures of Bence & Albee (1968) with modifications of Albee & Ray (1970). Synthetic and natural minerals were used as standards. Details of the microprobe procedures, uncertainties, and mineral recalculation routines have been reported by Clynne (1993).

The heterogeneity of the 1915 dacite lava and pumice required special treatment to obtain representative bulk-rock analyses. At least 0·5 kg of rock was broken to ~1 cm diameter fragments by hand, and any fragment containing macroscopic (>2 mm) andesitic inclusion was discarded. The remaining sample was crushed, split, and ground using conventional techniques. Major-element compositions were determined at the USGS Analytical Laboratory in Lakewood, Colorado, by wavelength-dispersive X-ray fluorescence analysis of fused glass disks (Taggart *et al.*, 1987). Minor elements (Rb, Sr, Ba, Y, Zr, Ni, and Cr) were determined at Menlo Park by energy dispersive X-ray fluorescence analysis (EDXRF) of finely ground rock powder by Peggy Bruggman. Precision of major- and trace-element analyses was determined by repeated analysis of internal standards (Bacon & Druitt, 1988).

LITHOLOGIC DESCRIPTIONS

In May 1915, four volcanic rock types erupted from Lassen Peak over a 3 day period. Black dacite lava
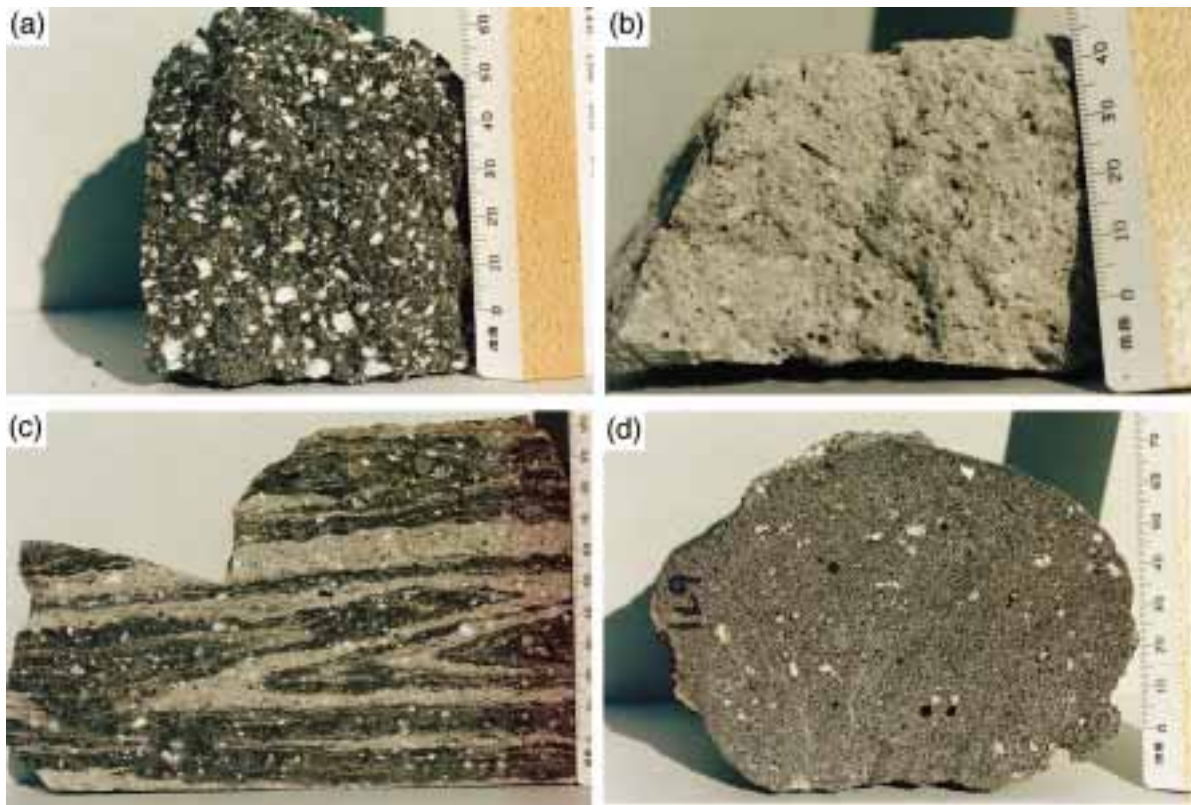
Plate 1. The rock types erupted from Lassen Peak in 1915: (a) black dacite from the lava dome erupted between May 14 and 19 resembles black dacite from the lava flow (shown here) erupted on May 19; (b) a small block of light dacite pumice erupted on May 22; (c) sawn slab of compositionally banded pumice erupted on May 22; (d) sawn andesitic inclusion. (Note the partially reacted phenocrysts, the coarse and even-textured grain size of the groundmass, and the lack of crenulate margins on the andesitic inclusion.)

formed the dome that grew between May 14 and 19 and the flow (Plate 1a) emplaced on May 19–20. Light dacite pumice occurs as unlayered blocks (Plate 1b) and in compositionally interlayered blocks with dark andesite pumice (Plate 1c) that were both erupted on May 22. Andesitic inclusions (Plate 1d) of undercooled hybrid magma are present in both the black dacite and light dacite. Elsewhere, the latter rock type has been termed 'magmatic or mafic inclusions', 'enclaves', 'blobs', or 'quenched inclusions' (e.g. Heiken & Eichelberger, 1980; Bacon, 1986; Linneman & Myers, 1990; Koyaguchi & Blake, 1991). Here, the inclusions are termed 'andesitic' to reflect their compositional affinity. The terms black dacite, light dacite, and dark andesite are used merely to describe the eruption products. The black dacite, light dacite, and dark andesite contain coexisting populations of unreacted and reacted phenocrysts that are described in detail below.

Black dacite

The lava dome and flow (64–65 wt % SiO_2), are similar in appearance and composition. Both are coarsely porphyritic and contain large plagioclase, biotite, horn-blende, and quartz phenocrysts in a microvesicular groundmass of abundant clear, light brown glass with microphenocrysts of plagioclase, clinopyroxene, ortho-pyroxene, and titanomagnetite. Small olivine phenocrysts with thin reaction rims of orthopyroxene are also present. The black dacite contains abundant andesitic inclusions that range from a few millimeters to 50 cm in diameter. Lava of the dome contains more small fragments of andesitic inclusions than does the lava flow.

A small volume of black dacite occurs as dense glassy lithic blocks in the deposits of banded and light pumice. Most of these blocks contain ~63 wt % SiO_2 and are slightly more mafic than the dome and flow lava (Clynne, 1993). Except for their nonvesicular groundmass and a larger proportion of plagioclase and pyroxene micro-phenocrysts and olivine phenocrysts, the blocks are pet-rographically identical to the black dacite of the dome and flow. These lithic blocks are interpreted as fragments of degassed, solidified magma that filled the volcanic conduit which fed the lava dome and flows before the pyroclastic eruption of May 22. They are slightly more mafic than typical black dacite because they contain tiny fragments of inclusions that could not be removed during sample preparation.

Light dacite

Light dacite, the most silicic of the 1915 rock types (64·5–68 wt % SiO_2), also varies the most in composition. In May 22 deposits, it occurs as light bands in the banded pumice and as vaguely banded to unbanded material. Unbanded blocks as long as 10 m probably represent unmingled light dacite magma. Some banding appears blobby.

Some light dacite is compositionally equivalent to black dacite, and its phenocryst assemblage and abundance resembles that of black dacite. The most silicic light dacite has nearly 68 wt % SiO_2, and is less porphyritic than the black dacite. Most light dacite is intermediate between these two composition end members. Small andesitic inclusions, olivine phenocrysts, reacted plagioclase, amphibole, biotite, and quartz phenocrysts, and clinopyroxene, orthopyroxene, plagioclase, and titanomagnetite microphenocrysts decrease with increasing SiO_2 content of light dacite. The ratio of unreacted to reacted phenocrysts in light dacite increases with SiO_2 content.

Dark andesite

Typically, even the thickest dark andesite bands display blebs and streaks of light dacite. The scale of banding varies from a few millimeters or centimeters (Plate 1c), to meter-sized blocks that display predominantly light or dark bands. The least contaminated dark andesite contains olivine phenocrysts in a dark glassy groundmass with tiny pyroxene and plagioclase microphenocrysts. Phenocrysts range from unreacted to strongly reacted. However, strongly reacted phenocrysts are less abundant in the dark andesite than in either the black dacite or the light dacite. Andesitic inclusions are rare, a few centimeters in length, and typically are smeared out along flow planes. The least contaminated dark andesite bands contain 60–61 wt % SiO_2.

Andesitic inclusions

Andesitic inclusions range up to ~50 cm in diameter and make up ~5–10% of the lava dome and flow. They are sparser and smaller in the light dacite than the black dacite and are scarcest in the most silicic light dacite. They are rare in the dark andesite, in which they appear to have been admixed from adjacent light dacite bands. The andesitic inclusions are glass rich and only rarely have the crenulated, finer-grained margins typically observed on undercooled inclusions (e.g. Bacon, 1986). Instead, most andesitic inclusions in the 1915 lava are subrounded to subangular and generally are broken. Their even-grained texture resembles that called 'coarse-grained' in Heiken & Eichelberger's (1980) description

of slower-cooled interiors of large inclusions at Chaos Crags.

The andesitic inclusions are gray to black. They contain phenocrysts of olivine in a microvesicular network of acicular and sometimes swallowtail or hollow plagioclase, clinopyroxene, and orthopyroxene microphenocrysts up to 0·5 mm long, with ~50% interstitial light to dark brown glass. Euhedral grains of titanomagnetite are an abundant accessory mineral. Most inclusions also contain a small amount of acicular hornblende, typically as a reaction product of acicular pyroxene, and up to 5–10% of strongly reacted phenocrysts of plagioclase, hornblende, biotite, and quartz. Reacted phenocrysts are evenly distributed throughout the inclusions. SiO_2 content of inclusions ranges from 57 to 59·5 wt % and increases with the abundance of reacted phenocrysts.

Groundmasses

The groundmass of the black dacite, dark andesite, and light dacite is hyalopilitic, whereas the groundmass of the andesitic inclusions is hyalo-ophitic. Glass generally constitutes about half the mode of the 1915 rock types. It is dark brown in dark andesite and andesitic inclusions, light brown in black dacite, and colorless in light dacite. Except for the most silicic light dacite, the glass in 1915 rocks is crowded with tiny unidentified microlites.

Acicular microphenocrysts of plagioclase, clinopyroxene, orthopyroxene, and blocky titanomagnetite similar in size and character to those in the andesitic inclusions are abundant in black dacite lavas and less so in light dacite. Microphenocrysts of amphibole, biotite, and quartz are also present in light dacite, but sparse in black dacite. The fragments of andesitic inclusions contain dark brown glass different in color and composition from that of the host rock. Except for the lithic blocks of dense, glassy black dacite lava that erupted with the banded pumice, 1915 rocks are microvesicular or pumiceous.

MINERALOGY OF THE 1915 ROCKS

The mineral assemblages of the 1915 rocks consist of three groups (see Table 1). The first two were derived from a dacite that was the silicic component of the mixing array. They are: (1) unreacted phenocryst or microphenocryst phases (sodic plagioclase, biotite, low-Al amphibole, Fe-rich orthopyroxene, quartz, and low-Ti titanomagnetite); and (2) reacted populations of the same phenocrysts (including two populations of sodic plagioclase but excluding Fe-rich orthopyroxene, which was not significantly reacted). The third group consists of phenocryst or microphenocryst phases derived from the mafic component of the mixing array (olivine, clinopyroxene, Mg-rich orthopyroxene, two populations of

Table 1: Occurrence and relative abundance of mineral populations in the 1915 rock types

	Black dacite	Light dacite	Dark andesite	Andesitic inclusions
Phenocrysts and microphenocrysts derived from the silicic component				
Plagioclase (sodic)				
unreacted* unzoned	A	A	S	—
microphenocrysts*	R	R	—	—
strongly reacted	C	C	S	C
weakly reacted	—	—	C	—
Amphibole (low-Al)				
unreacted	C	C	R	—
reacted	S	S	R	S
Biotite				
unreacted	C	C	R	—
reacted	S	S	R	S
Quartz				
unreacted	C	C	R	—
reacted	S	S	R	S
Fe-rich enstatite	S	S	R	R
Titanomagnetite (low-Ti)				
unreacted	S	S	R	—
reacted	R	R	R	R
Phenocrysts and microphenocrysts derived from the mafic component				
Olivine	S	S	C	C
Mg-rich augite	C	C	S	A
Mg-rich enstatite	C	C	S	A
Plagioclase (calcic)				
strongly zoned microphenocrysts	C	C	S	A
weakly zoned microphenocrysts	—	—	S	—
Titanomagnetite (high-Ti)	C	C	S	A
Amphibole (high-Al)	R	R	R	S

*Unreacted phenocrysts and unzoned microphenocryts in the black dacite and light dacite are compositionally equivalent and form a single population.

A, abundant; C, common; S, sparse; R, rare; —, absent.

calcic plagioclase, high-Al amphibole, and high-Ti titanomagnetite). Although both reacted and unreacted phenocrysts coexist in the black dacite and light dacite, the andesitic inclusions contain only reacted phenocrysts. Weakly reacted sodic plagioclase phenocrysts and weakly zoned plagioclase microphenocrysts are confined to the dark andesite. Chromian spinel is present as inclusions in olivine phenocrysts in all 1915 rocks. The accessory phases apatite and zircon are present and mostly easily observed as inclusions in large phenocrysts.
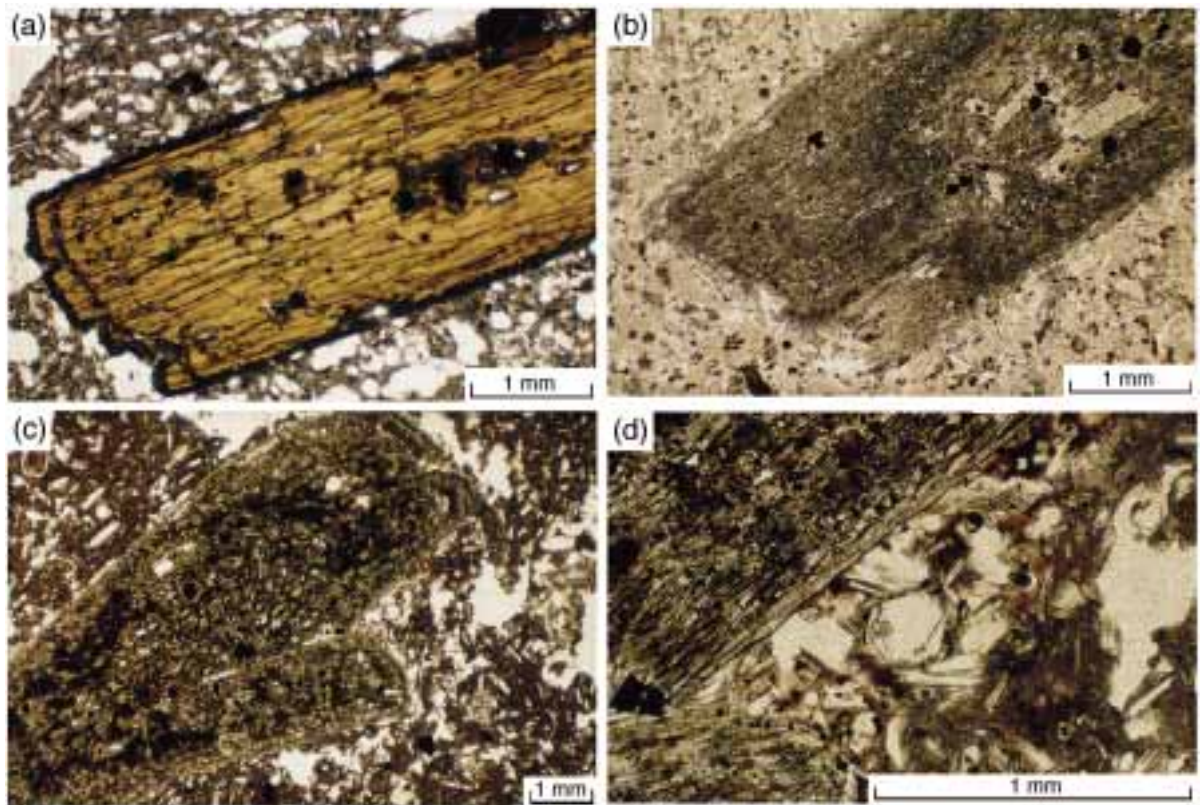
Amphibole

Amphibole occurs as sparse phenocrysts from 1 to 12 mm in size. It forms ~1% of the black and light dacite, and is less abundant in the andesitic inclusions and rare in the dark andesite. Unreacted amphibole displays light yellow–brown to reddish brown pleochroism, whereas partially reacted amphibole is pleochroic in dark reddish brown colors. In the black and light dacite, unreacted amphibole phenocrysts typically display thin (10–50 μm) rims of fine-grained plagioclase, pyroxene, and Fe–Ti oxide (Plate 2a). The extent of rim development anticorrelates with vesicularity in that amphibole phenocrysts in the most vesiculated pumice have thin rims or lack rims. Such features probably reflect volatile loss during ascent of magma in a conduit (Rutherford & Hill, 1993).

Reacted amphibole phenocrysts are partially to completely replaced by acicular pyroxene, fine-grained oxide, and plagioclase (Plate 2b–d). Ragged cores of amphibole are preserved in some relict crystals, but most are complete pseudomorphs for which only relict amphibole morphology indicates the original mineralogy. The correspondence of *c*-axes between replacement pyroxene and original amphibole suggests a replacement reaction, and is common in lavas that display other evidence of magma mixing (Mazzone *et al.*, 1987). It also suggests a rapid temperature rise in the host magma. Reacted and unreacted amphibole phenocrysts occur together in the black dacite, light dacite, and dark andesite, but only reacted amphibole phenocrysts are present in the andesitic inclusions. Small amphibole microphenocrysts in the groundmass of andesitic inclusions are probably reaction products of olivine phenocrysts or pyroxene microphenocrysts with residual liquid.

Large unreacted amphibole phenocrysts in the light dacite and black dacite are unzoned magnesiohornblende (Table 2; nomenclature of Leake, 1978). They contain low Al_2O_3 (6 wt %) and low Na_2O and TiO_2 (1·1–1·2 wt %), and have *mg*-number of 80. Amphibole microphenocrysts from the andesitic inclusions are normally zoned magnesiohastingsite. They contain 12 wt % Al_2O_3 and 2–3 wt % each of Na_2O and TiO_2, and range in *mg*-number from 74 to 86.

Plagioclase

The black dacite contains ~20% plagioclase phenocrysts. Most are 3–5 mm, euhedral to subhedral crystals (Plate

Plate 2. (a) Amphibole phenocryst in black dacite erupted on May 19. The crystal has a thin reaction rim, and is typical of virtually unreacted phenocrysts in the 1915 rocks. The thickness of the reaction rim is typically less in the banded pumice than in the lavas, and generally is absent in the light dacite. (b) Reacted amphibole phenocryst in an andesitic inclusion from the black dacite. This is almost a complete pseudomorph that consists of an aggregate of acicular pyroxene that is arranged parallel to the prismatic section of the amphibole crystal, fine-grained oxide, and plagioclase. Some small patches of amphibole are preserved in cores of this type of reacted crystal. (c) Reacted amphibole phenocryst in the black dacite. This crystal is similar to that shown in (b) but very different from that shown in (a). (d) Detail of the area between the intergrown crystals shown in (c). A small piece of andesitic inclusion adheres to the reacted amphibole. It is readily identified by the olivine microphenocryst and the textural arrangement of acicular pyroxene, tabular plagioclase, and clear brown glass identical to that in andesitic inclusions [compare with inclusion texture in (b)].

3a), but composite crystals up to ~12 mm are conspicuous. Unreacted plagioclase phenocrysts are clear and display oscillatory zoning. Most are about An_{30} in composition, but zones or cores to about An_{45} are common (Table 3; Fig. 1). Rarely, unreacted phenocrysts display ragged xenocrystic cores as calcic as An_{80}. Rims a few tens of microns thick that range from the core composition to about An_{50} occur on unreacted plagioclase phenocrysts. Calcic rims are better developed and range to higher An content on unreacted phenocrysts in the black dacite than on counterparts in light dacite. Larger, unreacted plagioclase phenocrysts have patchy zoned cores and smeared or partially recrystallized oscillatory areas with a thin calcic outer zone. Such crystals record partial reaction of the phenocryst which was later obscured by recrystallization (see description of reacted plagioclase phenocrysts below) and subsequently overgrown by calcic plagioclase. These textures testify to a long, complex

history of growth punctuated by magma mixing events.

Approximately 20–30% of plagioclase phenocrysts in black dacite (Plate 3d and e), a smaller percentage in light dacite, and all the plagioclase phenocrysts in the andesitic inclusions (Plate 3b and c) display varied but significant degrees of reaction. Reacted crystals are clouded (fritted) with small glass inclusions (Macdonald & Katsura, 1965). The clouded parts of the crystals are typically rounded. Commonly the entire crystal is clouded, but larger phenocrysts often preserve a ragged remnant of clear plagioclase (Plate 3b). Tsuchiyama (1985) experimentally reproduced this texture. He concluded that it arises from partial melting of plagioclase crystals that are placed into a hotter liquid which requires a significantly more calcic equilibrium plagioclase composition.

The composition of the ragged cores of reacted phenocrysts and the zoning patterns preserved in them resemble

Table 2: Representative analyses of amphibole in 1915 rock types

	Andesitic inclusion		Light dacite	
	mpc	mpr	phc	rem ph
SiO_2	42·65	42·92	49·59	49·12
Al_2O_3	13·12	11·42	6·05	6·54
FeO	4·49	8·28	7·30	7·93
Fe_2O_3*	6·32	3·92	5·05	4·89
MgO	15·42	14·46	16·28	15·90
MnO	0·13	0·17	0·54	0·56
TiO_2	2·11	2·75	1·04	1·11
CaO	11·23	11·33	11·59	11·61
Na_2O	2·15	2·41	1·10	1·27
K_2O	0·34	0·42	0·32	0·36
Cr_2O_3	0·01	0·01	0·00	0·00
F	0·16	0·32	0·18	0·19
Cl	0·01	0·03	0·04	0·05
Total	98·14	98·44	99·08	99·53
Si	6·131	6·249	7·055	6·982
$Al_{(IV)}$	1·869	1·751	0·945	1·013
$Al_{(VI)}$	0·354	0·210	0·069	0·085
Fe^{2+}	0·540	1·009	0·869	0·944
Fe^{3+}	0·683	0·429	0·541	0·523
Mg	3·303	3·138	3·453	3·370
Mn	0·016	0·021	0·065	0·067
Ti	0·228	0·301	0·111	0·118
Cr	0·002	0·001	0·000	0·000
Ca	1·730	1·768	1·767	1·770
Na	0·600	0·680	0·303	0·350
K	0·063	0·078	0·059	0·065
Total cations	15·518	15·634	15·237	15·286
mg-no.	86	76	80	78
Name	mght	mght	mghb	mghb

*Iron divided so that Fe_2O_3 is midway between the maximum and minimun permissible values (Papike *et al.*, 1974).
mpc, microphenocryst core; mpr, microphenocryst rim; phc, phenocryst core; rem ph, remnant core of reacted phenocryst; mght, magnesiohastingsite; mghb, magnesiohornblende.

those of the clear plagioclase phenocrysts (Table 3; Fig. 1a, c and d), although the former tend to be slightly more calcic. Reacted crystals have a clear rim of 0·05–0·1 mm thickness (henceforth called an overgrowth rim) of more calcic plagioclase that tends to restore the euhedral outline of the crystal. Overgrowth rims display strong normal zoning, generally from about An_{75} at the boundary with the reacted area to about An_{50} at the crystal margin (Fig. 1a–c). The outer margins of overgrowth rims on reacted plagioclase phenocrysts in silicic light dacite have abnormally high Or contents (Fig. 1d), apparently as a result of reaction with the relatively K-rich, light dacite magma. Overgrowth rims contain small pyroxene or titanomagnetite microphenocrysts identical to those in the groundmass of andesitic inclusions (Plate 3c and e). Similar overgrowth rims are produced experimentally by cooling after a mixing event in which the An content of the equilibrium plagioclase has been increased (Tsuchiyama, 1985).

The dark andesite also contains a second population of reacted plagioclase phenocrysts. These display the same core composition and zoning pattern as both un-reacted and strongly reacted phenocrysts (Fig. 1a–d), but evidence for reaction is confined to the margin of the phenocryst in a zone a few tenths of a millimeter wide. These weakly reacted plagioclase phenocrysts have rims of clear plagioclase that grew after reaction, are more calcic than the cores, and are weakly, normally zoned in the range An_{40-60}. These rims are less calcic than the overgrowth rims on strongly reacted plagioclase pheno-crysts, but more calcic than the rims on unreacted phenocrysts (Fig. 1b–d).

Acicular plagioclase microphenocrysts up to ~0·5 mm in length occur in all rock types. They are the most abundant phase in andesitic inclusions. The micro-phenocrysts display small cores of about An_{75} composition and strong normal zoning to about An_{50} at their rims. The latter mimic the zoning pattern of overgrowth rims on reacted phenocrysts (Fig. 1a–d). Microphenocrysts similar in composition to the unreacted phenocrysts (An_{30-40}) are sparse in light dacite and rare in dark andesite and black dacite. The dark andesite also contains blocky microphenocrysts similar in composition to the acicular microphenocrysts, but which lack small calcic cores.

Quartz

Quartz phenocrysts make up <1% of each rock type, and are rarest in the dark andesite. These phenocrysts range from 1 to 6 mm, but the smaller grains are crystal fragments. Unreacted crystals are rounded, embayed, and cracked, but have sharp boundaries and lack evidence for reaction with groundmass. Apatite grains and fluid inclusions are common in quartz phenocrysts. The latter generally contain fluorite daughter crystals (Williams, 1932) and vapor bubbles.

Reacted quartz grains are surrounded by rims that consist of fine-grained clinopyroxene in brown glass. The clinopyroxene crystals radiate from the former host liquid–brownish glass interface toward the quartz pheno-cryst. The degree of rim development is variable, but a quartz core is usually present. Reacted quartz phenocrysts are found in all rock types, but are conspicuous in the
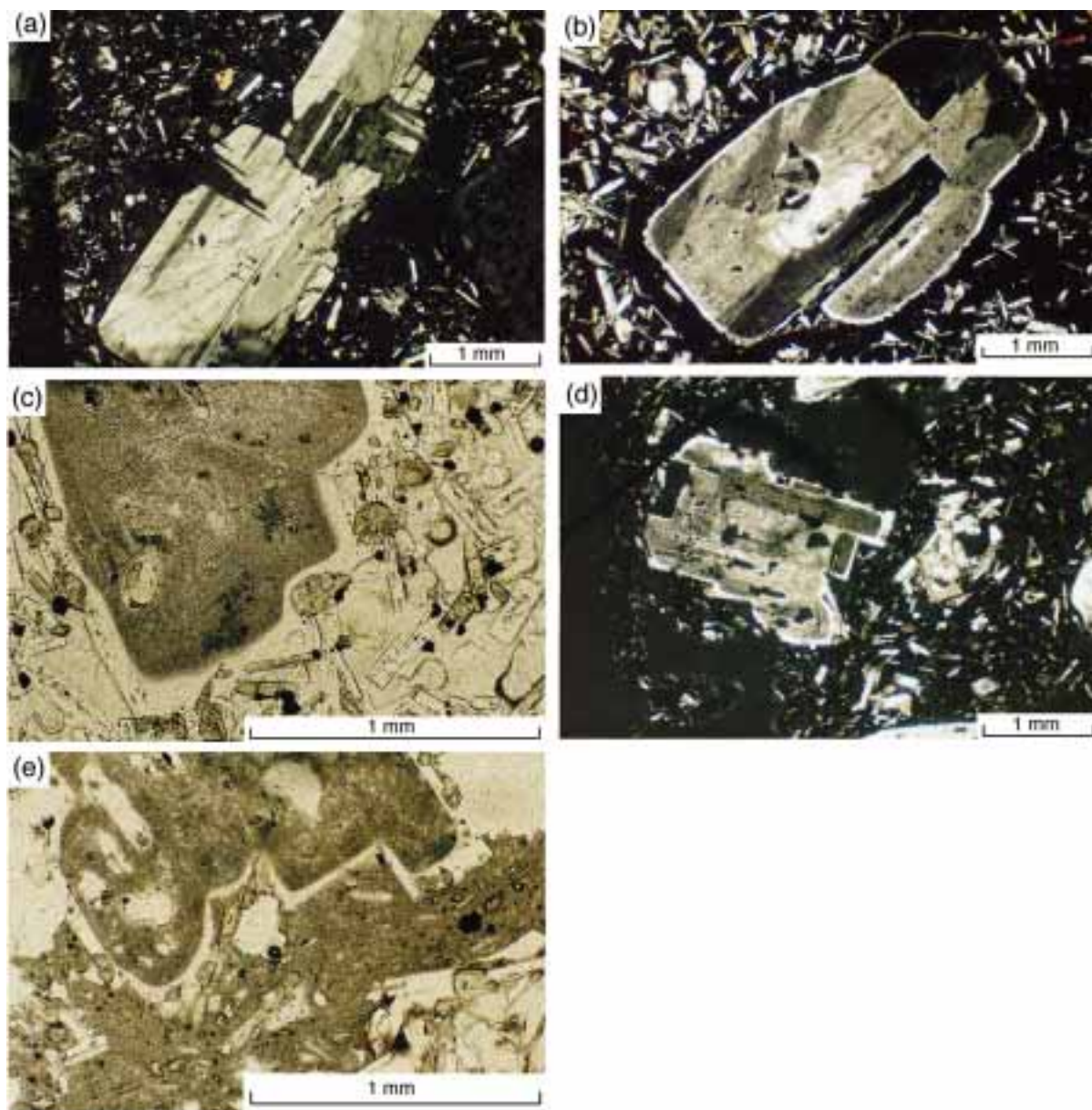
Plate 3. (a) Plagioclase phenocryst in black dacite erupted on May 19. The majority of plagioclase phenocrysts in all rock types except andesitic inclusions are unreacted and are of andesine composition. Some unreacted plagioclase crystals, like this one, display oscillatory and normal zoning without significant breaks or reversals. Other crystals display features such as normal and reverse zoning, healed reaction events, and patchy zoned or calcic cores. Thin (0·01 mm or less) rims more calcic than the core are typically present, but are not visible in this photograph. (b) Plagioclase phenocryst in an andesitic inclusion from the black dacite. Plagioclase phenocrysts in the inclusions are always strongly reacted. The reaction may extend completely or nearly completely through the crystal, leaving ragged patches of clear feldspar in the core. The reacted portions of the plagioclase crystals consist of: (1) fine-grained intergrowths of plagioclase more calcic than the original crystal; and (2) glass, probably of sodic plagioclase composition. Plagioclase phenocrysts in the andesitic inclusions always have a clear strongly zoned 0·1 mm overgrowth rim of plagioclase more calcic than the phenocryst and of the same composition as the plagioclase microphenocrysts in the inclusion groundmass. (c) Detail of a reacted plagioclase phenocryst in an andesitic inclusion. (Note the clinopyroxene microphenocrysts included in the clear overgrowth rim, indicating that the rim formed after reaction and simultaneously with crystallization of the inclusion groundmass.) (d) Reacted plagioclase phenocryst in the black dacite. Approximately 20% of the plagioclase phenocrysts in the black dacite and a smaller percentage in the light dacite are reacted. These crystals show all the features of the reacted plagioclase in the andesitic inclusions. (e) Detail of plagioclase phenocryst in (d). (Note the clinopyroxene microphenocrysts in the overgrowth rim, similar to those in the andesitic inclusions, indicating that this plagioclase phenocryst was released from an andesitic inclusion.)


Columns: Andesitic inclusion: rpc, og-i, og-o, mpc, mpa, mpr. Dark andesite: srpc, srog-i, srog-o, rpc, og-i, og-o, mpa, mpr.

Table 3: Representative analyses of plagioclase in the 1915 rock types

	Andesitic inclusion						Dark andesite							
	rpc	og-i	og-o	mpc	mpa	mpr	srpc	srog-i	srog-o	rpc	og-i	og-o	mpa	mpr
SiO₂	59·11	49·87	57·48	49·67	51·28	55·95	59·91	52·10	54·01	60·48	49·47	54·34	50·67	53·37
Al₂O₃	24·50	31·05	25·91	31·94	30·63	27·19	25·41	30·14	28·98	24·58	32·01	27·11	30·79	28·31
FeO	0·17	0·49	0·49	0·56	0·57	0·55	0·23	0·59	0·56	0·21	0·54	0·62	0·58	1·08
MgO	0·03	0·13	0·05	0·14	0·12	0·08	0·01	0·10	0·13	0·02	0·17	0·08	0·14	0·33
CaO	7·57	15·11	9·16	14·65	13·32	9·60	7·10	12·70	11·35	6·30	14·67	9·97	13·64	11·96
K₂O	0·45	0·08	0·36	0·10	0·13	0·30	0·49	0·18	0·25	0·59	0·11	0·24	0·11	0·26
Na₂O	7·25	3·23	6·37	3·42	4·10	6·48	7·20	4·16	4·84	7·68	3·05	5·66	3·64	4·41
SrO	0·12	0·09	0·17	0·12	0·12	0·16	0·13	0·10	0·12	0·08	0·13	0·15	0·19	0·10
Total	99·20	100·05	99·99	100·60	100·27	100·31	100·48	100·07	100·24	99·94	100·15	98·17	99·76	99·82
Si	2·667	2·282	2·587	2·260	2·331	2·520	2·663	2·366	2·438	2·698	2·258	2·500	2·316	2·426
Al	1·303	1·674	1·374	1·712	1·641	1·444	1·331	1·613	1·541	1·292	1·722	1·470	1·659	1·517
Fe	0·006	0·019	0·018	0·021	0·022	0·021	0·008	0·022	0·021	0·008	0·021	0·024	0·022	0·041
Ca	0·366	0·741	0·442	0·714	0·648	0·463	0·338	0·618	0·549	0·301	0·717	0·492	0·668	0·583
Na	0·634	0·287	0·556	0·302	0·362	0·566	0·620	0·366	0·424	0·665	0·270	0·505	0·322	0·388
K	0·026	0·005	0·021	0·006	0·007	0·017	0·028	0·010	0·014	0·034	0·006	0·014	0·007	0·015
Mg	0·002	0·009	0·003	0·009	0·008	0·005	0·001	0·007	0·008	0·002	0·012	0·005	0·009	0·022
Sr	0·003	0·002	0·004	0·003	0·003	0·004	0·003	0·003	0·003	0·002	0·004	0·004	0·005	0·003
An	35·7	71·8	43·4	69·9	63·7	44·3	34·3	62·1	55·6	30·1	72·2	48·7	67·0	59·1
Ab	61·85	27·8	54·6	29·5	35·5	54·1	62·9	36·8	42·9	66·5	27·1	50·0	32·3	39·4
Or	2·5	0·5	2·0	0·6	0·7	1·6	2·8	1·0	1·5	3·4	0·7	1·4	0·7	1·5
Sr (ppm)	1045	762	1399	976	1002	1321	1088	825	1044	694	1130	1127	1575	864

	Black dacite									Light dacite							
	pc	pr	xc	rpc	og-i	og-o	mpc	mpa	mpr	pc	pr	rpc	og-i	og-o	mpc	mpa	mpr
SiO_2	60.92	57.68	48.88	57.22	50.20	54.98	49.92	49.54	57.21	60.74	60.81	62.36	50.32	56.28	50.77	52.02	56.33
Al_2O_3	24.76	26.46	35.19	25.56	30.15	26.81	31.56	31.11	25.67	24.21	23.17	21.94	30.55	26.19	29.08	29.27	26.54
FeO	0.22	0.52	0.35	0.24	0.48	0.71	0.52	0.50	0.77	0.20	0.23	0.22	0.43	0.59	0.49	0.54	0.57
MgO	0.01	0.04	0.03	0.01	0.11	0.08	0.11	0.11	0.11	0.03	0.01	0.02	0.14	0.08	0.16	0.13	0.12
CaO	6.47	9.38	16.10	8.46	15.12	11.56	14.65	14.28	9.12	6.30	6.62	6.53	14.98	10.49	14.82	13.44	10.47
K_2O	0.57	0.46	0.07	0.41	0.09	0.37	0.10	0.10	0.67	0.56	0.54	0.60	0.12	0.42	0.10	0.14	0.38
Na_2O	7.78	6.14	2.52	7.12	3.30	5.19	3.40	3.64	5.85	7.64	7.29	8.19	3.23	5.18	3.51	4.05	5.40
SrO	0.10	0.15	0.15	0.07	0.16	0.15	0.10	0.14	0.15	0.08	0.05	0.12	0.13	0.10	0.15	0.12	0.12
Total	100.83	100.83	103.29	99.09	99.61	99.85	100.36	99.42	99.55	99.76	98.72	99.98	99.90	99.33	99.08	99.71	99.93
Si	2.696	2.575	2.169	2.598	2.308	2.498	2.275	2.280	2.587	2.712	2.742	2.784	2.304	2.554	2.344	2.376	2.543
Al	1.291	1.392	1.840	1.368	1.633	1.435	1.695	1.687	1.368	1.274	1.232	1.154	1.649	1.401	1.583	1.576	1.412
Fe	0.008	0.019	0.013	0.009	0.019	0.027	0.020	0.019	0.029	0.008	0.009	0.008	0.017	0.002	0.019	0.021	0.021
Ca	0.307	0.448	0.765	0.411	0.745	0.563	0.715	0.704	0.442	0.301	0.320	0.312	0.735	0.510	0.733	0.658	0.506
Na	0.667	0.531	0.217	0.626	0.295	0.457	0.300	0.325	0.513	0.662	0.637	0.709	0.287	0.456	0.314	0.359	0.473
K	0.032	0.026	0.004	0.024	0.005	0.021	0.006	0.006	0.039	0.032	0.031	0.034	0.007	0.024	0.006	0.008	0.022
Mg	0.001	0.003	0.002	0.001	0.007	0.005	0.007	0.007	0.007	0.002	0.000	0.001	0.010	0.006	0.011	0.009	0.008
Sr	0.003	0.004	0.004	0.002	0.004	0.004	0.003	0.004	0.004	0.002	0.001	0.003	0.004	0.003	0.004	0.003	0.003
An	30.5	44.6	77.6	38.7	71.3	54.1	70.0	68.1	44.5	30.3	32.4	29.6	71.4	51.5	69.6	64.2	50.6
Ab	66.3	52.8	22.0	59.0	28.2	43.9	29.4	31.4	51.6	66.5	64.5	67.2	27.9	46.0	29.8	35.0	47.2
Or	3.2	2.6	0.4	2.2	0.5	2.0	0.6	0.6	3.9	3.2	3.1	3.2	0.7	2.4	0.6	0.8	2.2
Sr (ppm)	876	1271	1271	598	1334	1271	821	1188	1250	717	386	1022	1138	870	1253	1038	1047

rpc, reacted phenocryst core; og-i, inner part of overgrowth rim on reacted phenocryst; og-o, outer part of overgrowth rim on reacted phenocryst; mpc, microphenocryst core; mpa, microphenocryst average; mpr, microphenocryst rim; srpc, slightly reacted phenocryst core; srog-i, inner part of overgrowth rim on slightly reacted phenocryst; srog-o, outer part of overgrowth rim on slightly reacted phenocryst; pc, unreacted phenocryst core; pr, unreacted phenocryst rim; xc, xenocryst core.
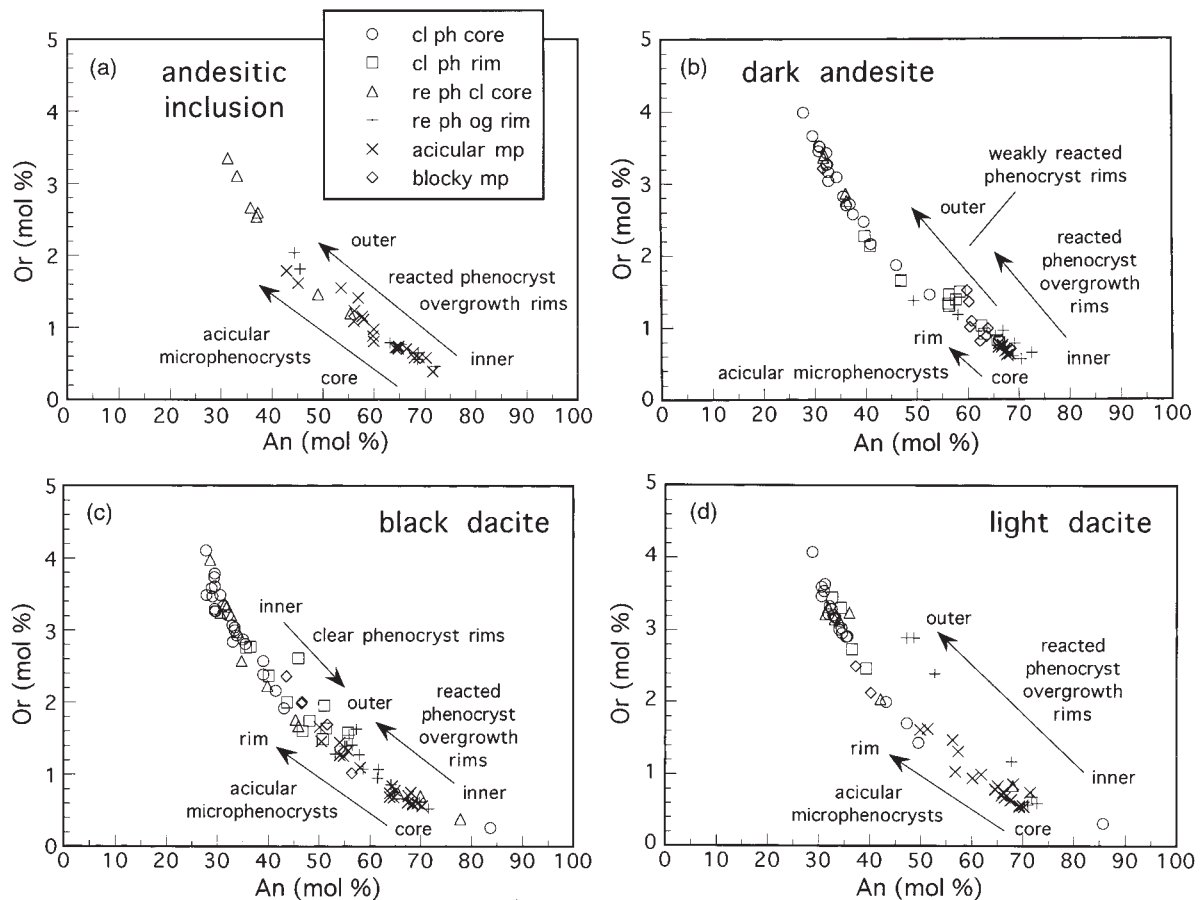
Fig. 1. Composition of plagioclase feldspars in the 1915 rock types plotted rectilinearly as mol % An vs mol % Or in the ternary system An–Ab–Or: (a) andesitic inclusions; (b) dark andesite; (c) black dacite; (d) light dacite. Symbols are indicated in the legend of (a), microphenocrysts include both core and average crystal compositions, and arrows indicate the range of core to rim zoning present in individual crystals. Abbreviations used include: ph, phenocryst; cl, clear; og, overgrowth; re, reacted; mp, microphenocryst. Unreacted plagioclase phenocrysts are oscillatory-zoned crystals of predominantly An_{30-40} plagioclase with thin rims as calcic as about An_{50}. Partially reacted plagioclase phenocrysts have relict oscillatory-zoned An_{30-40} cores and 0·1 mm thick overgrowth rims that have strong normal zoning from An_{75} to about An_{50}. Microphenocrysts have small calcic cores (An_{75}) and display strong normal zoning identical to the overgrowth rims on reacted phenocrysts. It should be noted that unreacted plagioclase phenocrysts and rims identical to those shown in (c) and (d) are present in the dark andesite but for clarity they are omitted from (b). Instead, the composition of weakly reacted phenocrysts and their rims are shown with open circles and squares, respectively. (See text for further discussion.)

andesitic inclusions and rare in the dark andesite. Quartz grains in the andesitic inclusions are the same size and shape as in the other rock types, but invariably display rims of clinopyroxene. The latter mineral is Mg-rich augite similar in Fe/Mg and Ca to that which occurs as microphenocrysts, but with other important differences in composition (see description of pyroxene, below).

Biotite

Biotite phenocrysts are present in each rock type. Euhedral to subhedral grains 1–3 mm across make up 1% of the black and light dacite. Fresh biotite crystals display dark greenish brown to light yellow–brown pleochroism. Biotite phenocrysts contain inclusions of apatite and zircon, and lack pleochroic halos around these minerals.

As with amphibole, biotite phenocrysts display both reaction rims and evidence for breakdown to anhydrous minerals. Biotite pleochroism becomes progressively darker and reddish brown with increasing rim thickness. Reacted biotite phenocrysts are replaced by a granular aggregate of pyroxene, titanomagnetite, ilmenite, and plagioclase, but sometimes have relict cores. In general, biotite is more extensively reacted than amphibole. Biotite is similar in composition to that reported by Heiken & Eichelberger (1980) from dacite of Chaos Crags.

Table 4: Representative analyses of olivine in 1915 rock types

	Andesitic inclusion		Dark andesite		Black dacite		Light dacite	
	phc	phr	phc	phh	phc	phr	phc	phr
SiO_2	39·17	38·69	39·56	38·61	39·60	38·55	39·72	38·97
MgO	45·07	43·50	44·41	42·37	44·77	42·15	44·67	42·19
FeO	15·41	17·09	15·56	17·82	15·45	19·01	15·47	18·17
MnO	0·25	0·26	0·23	0·28	0·25	0·31	0·25	0·29
NiO	0·34	0·25	0·31	0·15	0·32	0·25	0·33	0·18
CaO	0·11	0·11	0·13	0·17	0·12	0·12	0·11	0·15
Total	100·35	99·90	100·20	99·40	100·51	100·39	100·55	99·95
Si	0·985	0·983	0·996	0·977	0·994	0·986	0·996	0·995
Mg	1·690	1·648	1·666	1·598	1·674	1·607	1·669	1·605
Fe	0·324	0·363	0·328	0·377	0·324	0·406	0·325	0·388
Mn	0·005	0·005	0·005	0·006	0·005	0·006	0·005	0·007
Ni	0·007	0·005	0·006	0·003	0·007	0·005	0·007	0·004
Ca	0·003	0·003	0·003	0·005	0·003	0·003	0·003	0·004
Fo	83·9	81·9	83·6	80·9	83·8	79·8	83·7	80·5
Ni (ppm)	2672	1957	2436	1179	2491	1988	2617	1422

phc, phenocryst core; phr, phenocryst rim; phh, hopper overgrowth.

Olivine

Olivine is a phenocryst phase up to 0·8 mm in size in each rock type. It is most abundant in the andesitic inclusions and dark andesite, but even there makes up only 1–2% of the rock. Olivine is euhedral and typically contains sparse crystals of brownish chromian spinel. The cores of olivine phenocrysts in all rock types are unzoned Fo_{84} that averages 2300 ppm Ni and contains low CaO (Table 4, Fig. 2). Olivine crystals in the black dacite and andesitic inclusions have thin rims of olivine that are zoned to Fo_{80}. These rims are typically surrounded by a thin reaction rim of orthopyroxene and contain lower and more variable Ni than do phenocryst cores. In the black dacite and light dacite, olivine phenocrysts are typically found in 1–5 mm fragments of disaggregated andesitic inclusion groundmass (Plate 4a). Olivine phenocrysts in the dark andesite have the same composition as those in the black dacite, but occur as isolated euhedral crystals that display hopper overgrowths. The composition of overgrowths resembles that of the rims on olivine phenocrysts in the black dacite ($Fo_{84–80}$).

The continuous zoning profile of olivine phenocryst rims (including Ni content) suggests that they formed early in the crystallization of the andesitic inclusions. Near liquidus temperatures, Mg-rich olivine is stable in liquids that contain up to 63 wt % SiO_2 (Ussler, 1988). Orthopyroxene rims on olivine phenocrysts probably formed after significant cooling of the andesitic magma.

The orthopyroxene rims, along with pyroxene and plagioclase microphenocrysts that adhered to the olivine phenocrysts probably armored the latter from rapid reaction with the silicic magma. Hopper overgrowths on otherwise euhedral olivine phenocrysts in the dark andesite indicate that this rock type had a different cooling history from the andesitic inclusions.

Chromian spinel

Euhedral octahedra of brownish spinel 10–20 μm in diameter occur as inclusions in olivine phenocrysts in all the rock types. These spinel inclusions are Cr and Mg rich with low Ti and Fe^{3+}, and their composition is identical in each rock type (Table 5, Fig. 3). The latter feature indicates that the cores of all olivine phenocrysts have a common history (Clynne & Borg, 1997).

Pyroxene microphenocrysts

Orthopyroxene microphenocrysts are about twice as abundant as those of clinopyroxene in all rock types. These acicular pyroxene microphenocrysts reach lengths of ~0·5 mm, display strong continuous normal zoning of up to ~10 mol % En around small magnesian cores, and have the same composition and zoning pattern. Complexly intergrown orthopyroxene and clinopyroxene
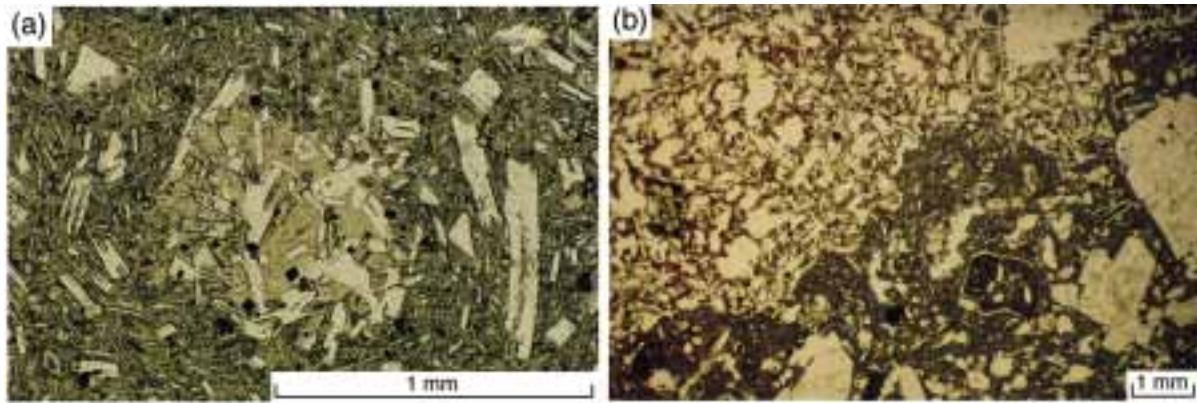
Plate 4. (a) Fragments of andesitic inclusions in the black dacite. Fragments of disaggregated andesitic inclusions are present in all other rock types, although sparse in the dark andesite. Solidification of the lava froze them into the groundmass while they were disaggregating on a crystal-by-crystal basis. Nearly all of the microphenocrysts visible in the lava groundmass originated from andesitic inclusions. Compare texture with Plates 2b and 3b. (b) The interface of an andesitic inclusion and the black dacite shows disaggregation of the inclusion into fragments and individual crystals.
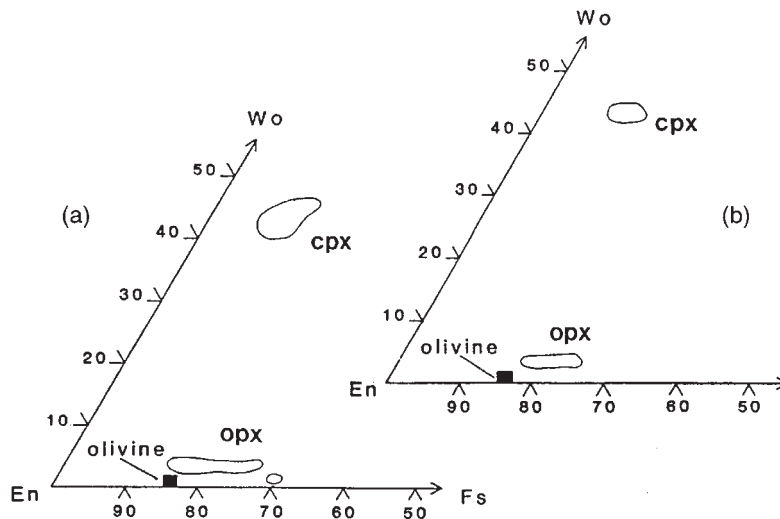
Fig. 2. Compositions of pyroxene and olivine in the 1915 rock types: (a) black dacite and light dacite; (b) andesitic inclusions. Andesitic inclusions, black dacite, and light dacite all contain acicular crystals of Mg-rich augite and enstatite zoned over a range of ~10 mol % En. Short stumpy prisms of unzoned Fe-rich orthopyroxene with lower Wo content are sparsely present in all 1915 rocks. Olivine occurs as unzoned Fo_{84} microphenocrysts with ~2400 ppm Ni and thin rims zoned to about Fo_{80}.

microphenocrysts occur in the andesitic inclusions, black dacite and light dacite.

Clinopyroxenes are Mg-rich augite (Morimoto *et al.*, 1988) with compositions that range from $Wo_{42} En_{49}$ cores with Al_2O_3 up to 5 wt % and Cr_2O_3 up to 0·58 wt % to $Wo_{45} En_{42}$ rims with ~2 wt % Al_2O_3 and generally 0·03 wt % or less Cr_2O_3 (Table 6, Fig. 2). Mg-rich augite has quadrilateral component totals of generally between 85 and 90%; Fe^{3+} and Al make up the most abundant non-quadrilateral components.

Orthopyroxenes are enstatite with compositions that range from En_{82} cores with Al_2O_3 up to 3 wt % and Cr_2O_3 up to 0·38 wt % to En_{72} rims with ~1 wt % Al_2O_3

and generally 0·02 wt % or less Cr_2O_3. Mg and Cr contents correlate well, and Mg-rich enstatite generally contains between 90 and 95% quadrilateral components. Wo content is typically between 3 and 4 mol %, but it is variable and only weakly correlated with decreasing En. A few enstatite crystals in the black dacite show thin rims of low-Wo, En_{69-70} orthopyroxene that were not found on microphenocrysts in the andesitic inclusions.

A second population of orthopyroxene micro-phenocrysts occurs sparsely in each rock type, but is most abundant in the black dacite and light dacite (although at most only a few crystals per thin section). The micro-phenocrysts are stumpy prisms of Fe-rich enstatite which,

Table 5: Representative analyses of chromian spinel included in olivine in the 1915 rock types

	Andesitic inclusion	Dark andesite	Black dacite	Light dacite
SiO_2	0·03	0·03	0·00	0·00
TiO_2	1·10	1·19	1·01	0·94
Al_2O_3	22·05	21·15	22·48	22·57
Cr_2O_3	31·27	30·73	32·27	32·08
FeO	20·29	19·32	20·20	19·60
Fe_2O_3*	14·10	15·78	13·70	13·96
MnO	0·38	0·23	0·23	0·23
MgO	10·59	11·16	10·81	11·04
Ni	0·09	0·32	0·24	0·26
CaO	0·01	0·01	0·00	0·01
V_2O_3	0·25	0·29	0·24	0·20
Total	100·16	100·21	101·18	100·89
Si	0·001	0·001	0·000	0·000
Ti	0·026	0·028	0·023	0·022
Al	0·816	0·782	0·821	0·825
Cr	0·779	0·765	0·794	0·790
Fe^{2+}	0·532	0·507	0·523	0·508
Fe^{3+}	0·333	0·372	0·319	0·326
Mn	0·007	0·006	0·006	0·006
Mg	0·493	0·522	0·500	0·511
Ni	0·007	0·008	0·006	0·006
Ca	0·000	0·000	0·000	0·000
V	0·006	0·007	0·006	0·005
mg-no.	48·1	50·8	48·9	50·1
cr-no.	48·8	49·4	49·2	48·9
Fe^{2+}/Fe^{3+}	1·60	1·36	1·64	1·56

*Fe_2O_3 calculated by charge balance and stoichiometry.
cr-no. = 100Cr/(Cr + Al), atomic.

Fig. 3. Chromian spinel octahedra included in olivine microphenocrysts display a small range of composition in *cr*-number [100Cr/(Cr + Al)] and *mg*-number space when compared with basalts and magnesian basaltic andesites from the Lassen area. [Note the lack of overlap between low-K olivine tholeiite (LKOT) and 1915 chromian spinel compositions, and the correspondence between the composition of spinel in calc-alkaline basalt and basaltic andesite (CAB) and 1915 rock types.]

component totals as a result of higher SiO_2 and lower Al_2O_3, Fe_2O_3, Cr_2O_3, and TiO_2.

in contrast to the acicular orthopyroxenes, are unzoned and display a narrow range of composition. These $En_{68–69}$ microphenocrysts contain 97–98% quadrilateral components, 1·2–1·4 mol % Wo, 0·6 wt % Al_2O_3, and lack Cr_2O_3.

In addition to the acicular pyroxene microphenocrysts found in andesitic inclusions and black dacite, the dark andesite contains 0·05–0·1 mm clinopyroxene and orthopyroxene microphenocrysts with blocky habit. The blocky microphenocrysts lack intergrowth textures. Although they have similar compositions to the acicular ones, the blocky microphenocrysts are not strongly zoned. The clinopyroxene from the reaction rims around quartz crystals are similar in composition to the acicular microphenocrysts (Table 6), but have higher quadrilateral
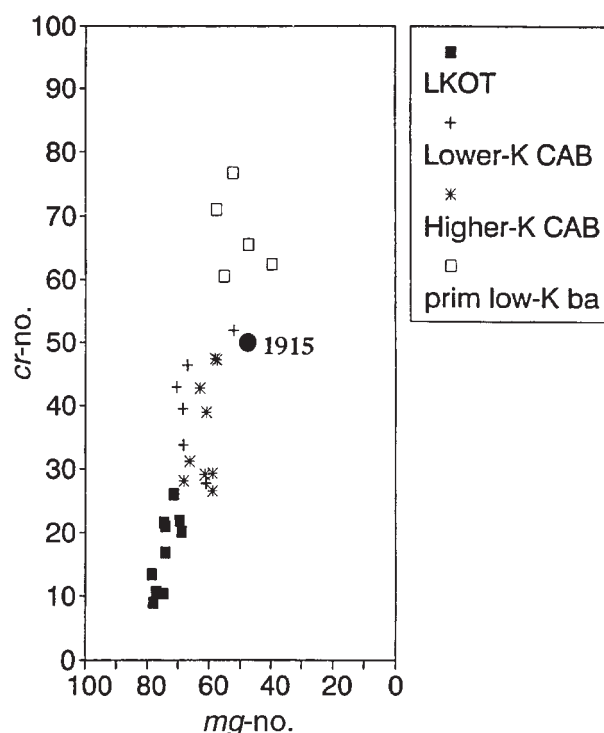
Titanomagnetite

Titanomagnetite phenocrysts and microphenocrysts are found in each rock type. Three types of titanomagnetite are distinguished by their ulvöspinel and Al_2O_3 contents (Table 7, Fig. 4). Euhedral microphenocrysts (maximum size 0·10 mm) of high-Ti titanomagnetite that range in composition from $Usp_{25–40}$ with 2–3·5 wt % Al_2O_3 are abundant in the andesitic inclusions, and less so in the other rock types. Phenocrysts of titanomagnetite up to 0·35 mm in diameter are present in all rock types. Most titanomagnetite phenocrysts have low-Ti compositions in the range $Usp_{14–17}$, with 1·3–1·8 wt % Al_2O_3. A second population of titanomagnetite phenocrysts and rims on some low-Ti titanomagnetite grains contain up to Usp_{30}, with 1·8–3·5 wt % Al_2O_3. Low-Ti phenocrysts occur in all rock types except the andesitic inclusions, whereas high-Ti phenocrysts occur in all rock types.

Table 6: *Representative analyses of pyroxene in 1915 rock types*

	Andesitic inclusion				Light dacite					Black dacite					
	cpx	cpx	opx	opx	cpx	cpx	opx	opx	opx	cpx	cpx	cpx	opx	opx	opx
	mpc	mpa	mpc	mpa	mpc	mpa	mpc	mpa	Femp	mpc	mpa	qtz	mpc	mpa	Femp
SiO_2	51·57	51·76	53·58	53·91	51·40	51·40	53·25	52·16	52·48	50·71	51·18	54·00	53·30	52·52	54·00
Al_2O_3	3·12	2·06	2·50	1·56	2·98	2·86	2·22	2·36	0·53	3·83	2·79	0·54	2·61	2·95	1·16
FeO	6·35	7·31	11·50	14·88	5·61	7·04	9·71	11·88	18·95	4·19	6·14	6·98	10·86	13·49	18·80
Fe_2O_3*	0·70	2·57	0·60	0·59	2·09	1·11	1·99	3·14	0·54	2·60	2·02	0·28	1·94	1·70	0·00
MgO	15·60	13·96	28·06	26·12	15·80	15·60	28·46	27·34	24·35	16·39	15·45	16·70	28·30	26·11	23·80
MnO	0·20	0·28	0·30	0·37	0·20	0·25	0·28	0·37	1·20	0·16	0·26	0·21	0·30	0·39	0·88
TiO_2	0·59	1·08	0·25	0·27	0·56	0·56	0·23	0·27	0·16	0·54	0·59	0·15	0·24	0·34	0·16
Cr_2O_3	0·24	0·01	0·26	0·03	0·16	0·05	0·24	0·06	0·01	0·53	0·07	0·00	0·13	0·04	0·01
CaO	20·63	19·74	1·84	2·04	20·80	20·00	2·31	1·68	0·75	20·35	20·53	20·90	1·73	1·96	0·80
Na_2O	0·30	0·41	0·03	0·07	0·29	0·27	0·05	0·02	0·02	0·32	0·32	0·21	0·03	0·04	0·09
Total	99·30	99·18	98·92	99·84	99·89	99·14	98·74	99·26	98·99	99·62	99·35	99·97	99·44	99·54	99·70
Si	1·913	1·833	1·929	1·953	1·899	1·915	1·918	1·893	1·959	1·870	1·904	1·988	1·911	1·905	1·985
$Al_{(IV)}$	0·087	0·134	0·071	0·047	0·101	0·085	0·082	0·101	0·023	0·130	0·096	0·012	0·089	0·095	0·015
$Al_{(VI)}$	0·049	0·030	0·036	0·020	0·028	0·041	0·012	0·000	0·000	0·036	0·027	0·011	0·002	0·031	0·036
Fe^{2+}	0·197	0·253	0·346	0·451	0·173	0·219	0·292	0·361	0·592	0·129	0·191	0·215	0·326	0·409	0·578
Fe^{3+}	0·019	0·073	0·016	0·016	0·058	0·031	0·054	0·086	0·015	0·072	0·057	0·008	0·052	0·046	0·000
Mg	0·863	0·781	1·506	1·410	0·870	0·866	1·528	1·479	1·354	0·901	0·857	0·916	1·513	1·412	1·304
Mn	0·006	0·009	0·009	0·011	0·006	0·008	0·009	0·011	0·038	0·005	0·008	0·007	0·009	0·012	0·027
Ti	0·016	0·031	0·007	0·007	0·016	0·016	0·006	0·007	0·004	0·015	0·016	0·004	0·006	0·009	0·004
Cr	0·007	0·000	0·007	0·001	0·005	0·001	0·007	0·002	0·000	0·015	0·002	0·000	0·004	0·001	0·000
Ca	0·820	0·794	0·071	0·079	0·823	0·798	0·089	0·065	0·030	0·804	0·819	0·824	0·006	0·076	0·032
Na	0·022	0·030	0·002	0·005	0·021	0·020	0·003	0·001	0·001	0·023	0·023	0·015	0·002	0·003	0·006
Quad %	90·8	86·6	92·9	95·3	89·3	91·1	91·8	89·9	97·7	86·2	89·8	97·7	91·1	90·5	96·0
Wo	43·6	43·4	3·7	4·1	44·1	42·4	4·7	3·4	1·5	43·8	43·9	42·2	3·5	4·0	1·7
En	45·9	42·7	78·3	72·7	46·6	46·0	80·0	77·7	68·5	49·1	45·9	46·9	79·4	74·4	68·2
Fs	10·5	13·9	18·0	23·2	9·3	11·6	15·3	18·9	29·9	7·1	10·2	11·0	17·1	21·6	30·2
mg-no.	81·4	75·5	81·3	75·8	83·4	79·8	84·0	80·4	69·6	87·5	81·8	81·0	82·3	77·5	69·3

*Fe_2O_3 calculated by method of Papike *et al.* (1974).
mpc, microphenocryst core; mpa, microphenocryst average; Femp, Fe-rich enstatite microphenocryst; qtz, clinopyroxene in rim on quartz phenocryst.

Table 7: Representative analyses of titanomagnetite in 1915 rock types

	Andesitic inclusion			Black dacite					Light dacite				
	rpc	rpr	mpc	pc	pr	rpc	rpr	mpc	pc	pr	rpc	rpr	mpc
MgO	1·82	2·35	2·79	1·25	1·55	1·42	2·07	1·27	1·45	1·82	2·05	2·04	2·21
Al_2O_3	1·69	3·80	2·56	1·52	1·78	1·48	2·72	2·75	1·62	2·94	2·06	2·58	2·47
SiO_2	0·00	0·01	0·00	0·00	0·00	0·00	0·00	0·07	0·00	0·00	0·00	0·00	0·00
CaO	0·00	0·02	0·01	0·02	0·00	0·00	0·04	0·03	0·01	0·06	0·02	0·05	0·04
TiO_2	5·46	8·21	11·31	5·03	5·98	4·96	9·82	10·89	5·45	8·24	6·31	8·67	9·44
V_2O_3	0·42	0·55	0·57	0·42	0·51	0·41	0·59	0·55	0·39	0·63	0·51	0·67	0·70
Cr_2O_3	0·10	0·18	0·01	0·07	0·06	0·07	0·09	0·03	0·07	0·11	0·08	0·10	0·17
MnO	0·39	0·39	0·45	0·52	0·43	0·63	0·43	0·47	0·55	0·47	0·38	0·44	0·43
NiO	0·02	0·01	0·01	0·00	0·04	0·05	0·03	0·02	0·00	0·07	0·05	0·03	0·01
FeO	33·75	35·59	37·34	33·86	34·66	33·50	37·40	39·38	33·85	36·12	33·85	35·87	36·38
Fe_2O_3*	58·12	49·95	45·22	58·43	56·96	58·98	48·25	44·91	57·46	50·53	55·34	49·48	48·17
Total	101·77	101·06	100·27	101·12	101·97	101·51	101·44	100·37	100·86	100·99	100·65	99·93	100·02
Mg	0·100	0·128	0·153	0·069	0·085	0·079	0·113	0·070	0·081	0·100	0·113	0·113	0·122
Al	0·073	0·163	0·110	0·067	0·077	0·065	0·117	0·120	0·071	0·127	0·090	0·113	0·108
Si	0·000	0·000	0·002	0·000	0·000	0·000	0·000	0·003	0·000	0·000	0·000	0·000	0·000
Ca	0·000	0·001	0·002	0·001	0·000	0·000	0·001	0·001	0·000	0·002	0·001	0·002	0·002
Ti	0·151	0·225	0·311	0·141	0·165	0·138	0·269	0·303	0·153	0·228	0·176	0·242	0·263
V	0·012	0·016	0·017	0·013	0·015	0·012	0·017	0·016	0·012	0·018	0·015	0·020	0·021
Cr	0·003	0·005	0·001	0·002	0·002	0·002	0·003	0·001	0·002	0·003	0·002	0·003	0·005
Mn	0·012	0·012	0·014	0·017	0·013	0·020	0·013	0·015	0·017	0·015	0·012	0·014	0·013
Fe^{2+}	1·038	1·082	1·143	1·054	1·065	1·038	1·141	1·219	1·054	1·109	1·048	1·113	1·125
Fe^{3+}	1·609	1·367	1·246	1·637	1·576	1·645	1·324	1·251	1·610	1·396	1·541	1·381	1·341
Ni	0·001	0·002	0·000	0·000	0·001	0·002	0·001	0·001	0·000	0·002	0·002	0·001	0·000
Usp	15	25	32	14	17	14	29	33	15	25	18	26	28

*Fe_2O_3 calculated by charge balance and stoichiometry.
pc, phenocryst core; pr, phenocryst rim; rpc, reacted phenocryst core; rpr, reacted phenocryst rim; mpc, microphenocryst core.
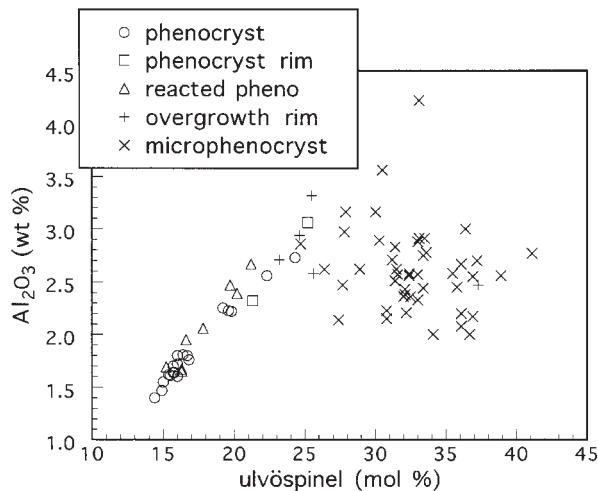
Fig. 4. Composition of titanomagnetite phenocrysts and microphenocrysts in the 1915 rock types plotted as mol % ulvöspinel vs wt % Al$_2$O$_3$. Titanomagnetites are plotted by composition groups instead of rock type. Two types of titanomagnetite phenocrysts and microphenocrysts are present in the rocks: (1) low-Ti (and low Al$_2$O$_3$) phenocrysts from the dacite end member are found in all rock types except the andesitic inclusions; (2) high-Ti (and high-Al$_2$O$_3$) microphenocrysts crystallized in the andesitic inclusions, and are found in all rocks. Low-Ti phenocrysts mixed into the andesitic-inclusion magma were partially reacted, and display overgrowth rims of high-Ti composition, and are also found in the dark andesite, black dacite, and light dacite.

MINERALOGY AND MAGMA MIXING

The best constraints upon the nature of magma mixing that produced the 1915 eruption products are the textures and compositions of plagioclase and pyroxene phenocrysts and microphenocrysts. Plagioclase best preserves these events because it is nearly ubiquitous in intermediate magmas, has a wide compositional range, and responds to changes in the composition of its host or in intensive parameters by changing its composition. However, the scenario based on data for plagioclase and pyroxene is also consistent with the other phases.

Plagioclase

The reacted and unreacted populations of plagioclase phenocrysts (and other phenocrysts) in the black dacite have distinct histories and thus could not have formed together. The similar composition and zoning pattern of plagioclase cores indicates that both textural types were originally a single population. However, the strong normal zoning of overgrowth rims on reacted phenocrysts contrasts sharply with the weakly zoned calcic rims on unreacted ones. The clear euhedral overgrowth rims on irregular-shaped reacted cores demonstrate that the reaction took place before crystallization of the inclusion groundmass began. The identical composition and zoning

pattern of overgrowth rims on reacted phenocrysts and the microphenocrysts indicates that both crystallized under identical conditions (Fig. 1). The acicular pyroxene and titanomagnetite microphenocrysts included within the plagioclase overgrowth rims show that these rims grew simultaneously with the groundmass of the andesitic inclusions (Plate 3b and e).

The dark andesite contains both strongly and weakly reacted plagioclase phenocrysts. Rims of the weakly reacted plagioclase phenocrysts are thinner, less zoned, and less calcic than those of strongly reacted plagioclase phenocrysts. Thus, weakly reacted plagioclase phenocrysts are essentially unreacted plagioclase phenocrysts with thicker and more calcic rims.

Clearly, the weakly reacted plagioclase phenocrysts in the dark andesite formed when their host magma interacted with a more mafic one. However, the thermal contrast between these magmas was evidently smaller than that between the host and contaminant magmas that produced the strongly reacted plagioclase phenocrysts. The intermediate composition of the calcic rims on the weakly reacted plagioclase phenocrysts indicates that the equilibrium composition of plagioclase following hybridization was more calcic in the dark andesite than in the black dacite and less calcic than the andesitic inclusions. The thickness and zoning of the rims indicates that, after thermal equilibrium was reached in the hybrid magmas, the amount of undercooling in the magma that produced the dark andesite was intermediate between those of the magmas that produced the andesitic inclusions and the black dacite.

Pyroxene

The strong normal zoning, complex intergrowths, and high tetrahedral Al content of the pyroxene microphenocrysts indicate that they grew rapidly at a high degree of undercooling (Lofgren, 1980). The high Cr content of crystal cores not only suggests that the andesitic inclusions had a mafic parent, but also indicates that the cores might have been small crystals in this parent. Because bulk-rock Cr content of the andesitic inclusions averages 60 ppm their mafic parent probably had 90–100 ppm Cr (see below). Some cores of clinopyroxene microphenocrysts contain 3600 ppm Cr (2600 ppm for orthopyroxene). The required mineral distribution coefficients are appropriate for equilibrium crystallization (Gill, 1981).

Although pyroxene geothermometry was attempted for clino- and orthopyroxenes, pyroxene pairs are not suitable for Lindsley–Anderson geothermometry for two reasons: (1) the rapid growth and strong zoning of the pyroxene microphenocrysts make selection of equilibrium pairs difficult; (2) the Lindsley–Anderson method requires pyroxenes to have <10 mol % nonquadrilateral components

(Lindsley & Anderson, 1983), and few clinopyroxene grains meet that requirement. Equilibrium was evidently not maintained during crystallization of the andesitic-inclusion groundmass.

The similar compositions, zoning, and intergrowth patterns of acicular pyroxene microphenocrysts indicate that they all crystallized in the andesitic inclusions, and that they were distributed into the other rock types and erupted before equilibrium with their new host magmas was established. The lack of zoning, low Wo content, and high quadrilateral component content of the Fe-rich orthopyroxene microphenocrysts indicates that they crystallized at a lower temperature than the other pyroxenes and probably under near-constant equilibrium conditions. The crystal-chemical evidence and modal abundance of Fe-rich orthopyroxene indicates that it crystallized in the silicic end member of the 1915 magmas.

Pyroxene rims on quartz phenocrysts

Augite rims on quartz phenocrysts form as a result of diffusion of Mg, Fe, and Ca into the zone of silicic liquid surrounding the quartz crystal (Ussler, 1988). Ussler (1988) noted that it was unlikely that the fragile-appearing rims on quartz crystals could grow and persist in a convecting magma, and proposed that such rims form after extrusion of the mixed magma. However, the presence of such rims on quartz in the andesitic inclusions from Lassen precludes their formation after extrusion. These formed when silicic magma that contained quartz phenocrysts mixed with mafic magma and then was undercooled. The growth of augite rims probably did not continue after the andesitic inclusions formed. Disaggregation of the andesitic inclusions released augite-rimmed quartz back into the host magma. Some augite rims on quartz phenocrysts are disrupted, but most are intact. This demonstrates that augite rims on quartz can survive some convection, but their presence nevertheless implies that eruption of the 1915 magma occurred soon after or during disaggregation of the inclusions.

Conclusions based on mineralogical observations

The unreacted phenocrysts (sodic plagioclase, quartz, amphibole, biotite, Fe-rich orthopyroxene, and low-Ti titanomagnetite) were derived from a 'host' dacite magma. The reacted equivalents of these phenocrysts formed when this magma mixed with a mafic magma that contained magnesian olivine (Tsuchiyama, 1985). After reaction, rapid cooling and crystallization of the hybrid magma produced the overgrowth rims on the reacted plagioclase phenocrysts. Simultaneously, the calcic plagioclase, Mg-rich augite, Mg-rich enstatite, and

high-Ti titanomagnetite microphenocrysts crystallized to form the groundmass of the andesitic inclusions. At some later time, the partially crystallized andesitic inclusions were disaggregated, and the reacted and overgrown phenocrysts and groundmass microphenocrysts were mixed with host dacite containing unreacted phenocrysts to produce the mineral assemblage of the black dacite and light dacite. The dark andesite probably represents mafic magma mixed with host dacite that was itself contaminated with disaggregated andesitic-inclusion groundmass (i.e. black dacite).

GEOCHEMISTRY

Fifty samples of 1915 rocks were analyzed and reported by Clynne (1993); representative analyses are given in Table 8. [See Clynne (1993) for the locality and stratigraphic context of each sample.] The samples of dark andesite and light dacite bands were selected for analysis based on minimal macroscopic mixing between bands. A few hybrid bands were also analyzed and found to have compositions intermediate between the dark and light bands.

Analytical data for 50 samples of the 1915 rocks (Clynne, 1993; Table 8) are presented as variation diagrams (Figs 5 and 6) for selected oxides and elements. SiO_2 ranges from 57 to 68 wt % and the data for other components plot as linear arrays in discrete groups by rock type, although fields for the black dacite and light dacite show considerable overlap. Data for Zr/Ba vs Rb/Sr form a curved array with the points falling in the same groups as in the variation diagrams (Fig. 7a). Addition of end-member compositions (see discussions below) significantly increases the curvature of the array. Zr/Ba vs Sr/Ba shows a linear array (Fig. 7b), and nearly all of the data lie in the same order as in Fig. 7a. Such patterns indicate a binary mixing relationship for all 1915 rocks.

End-member compositions

To demonstrate a mixing relationship for all 1915 rocks and estimate the composition of likely end members, the chemical data were fitted by linear regression (Clynne, 1993). Most components yield correlation coefficients >0·90. MgO and K_2O (Fig. 8a and b) illustrate the pattern for the major oxides, and Sr (Fig. 8c) illustrates that for the trace elements. The remarkably good fit of these data over a 10 wt % range in SiO_2 confirms the origin of all 1915 rocks by mixing, and projection of the mixing lines yields information on the compositions of possible end members.

Table 8: Major- and trace-element geochemistry of 1915 rock types

	Andesitic inclusion			Dark andesite		Black dacite					Light dacite			
Sample:	LC87-1232	LC89-1494	LC81-843	LC87-1207	LC81-846	LC86-1027*	LC86-954	LC86-1022	LC81-840	LC86-1028	LC81-841	LC85-727	LC86-955	LC86-986A
SiO_2	57·05	58·43	59·15	60·10	60·52	62·99	64·01	64·47	64·64	64·89	64·88	66·24	66·78	67·78
Al_2O_3	18·41	18·14	18·14	17·69	17·83	17·11	17·11	16·92	16·76	16·87	16·77	15·93	16·06	15·68
Fe_2O_3	1·33	1·24	1·18	1·15	1·10	0·97	0·90	0·84	0·86	0·83	0·86	0·84	0·77	0·73
FeO	4·78	4·46	4·25	4·15	3·98	3·49	3·24	3·03	3·12	3·00	3·13	3·03	2·76	2·62
FeO*	5·98	5·57	5·32	5·19	4·98	4·36	4·05	3·79	3·91	3·75	3·91	3·78	3·46	3·27
MgO	4·77	4·32	4·16	3·83	3·64	3·09	2·71	2·59	2·60	2·48	2·66	2·37	2·17	1·86
CaO	7·62	7·18	6·81	6·53	6·29	5·63	5·26	5·22	4·90	5·01	4·96	4·47	4·35	3·97
Na_2O	3·79	3·90	3·91	4·02	4·06	4·04	4·02	4·09	4·18	4·17	4·07	4·09	4·05	4·04
K_2O	1·31	1·44	1·49	1·64	1·68	1·90	2·01	2·13	2·17	2·06	2·13	2·36	2·39	2·64
TiO_2	0·71	0·66	0·63	0·63	0·62	0·55	0·52	0·50	0·51	0·48	0·50	0·47	0·46	0·49
P_2O_5	0·16	0·15	0·14	0·16	0·15	0·15	0·14	0·14	0·13	0·13	0·13	0·13	0·13	0·14
MnO	0·10	0·09	0·09	0·09	0·09	0·07	0·07	0·07	0·07	0·07	0·07	0·07	0·06	0·06
Total	99·39	99·79	99·74	99·50	99·80	99·38	99·35	99·28	99·63	99·56	99·56	99·18	98·99	98·84
LOI	0·02	0·07	0·01	0·01	0·06	0·04	0·10	0·25	0·04	0·13	0·16	0·64	0·57	0·49
FeO*/MgO	1·25	1·29	1·27	1·36	1·36	1·41	1·50	1·46	1·49	1·51	1·47	1·60	1·59	1·76
Rb (ppm)	31	34	40	41	47	55	51	58	58	48	59	62	73	71
Sr	578	536	539	497	484	475	432	463	434	434	432	394	348	352
Ba	388	433	448	486	489	567	598	606	657	598	616	647	717	674
Y	16	13	15	18	15	17	15	16	15	17	13	16	16	14
Zr	96	100	107	105	113	117	115	133	121	116	120	125	133	133
Ni	56	48	53	41	49	31	26	n.d.	28	22	24	n.d.	17	23
Cr	74	53	58	51	62	34	26	n.d.	26	14	20	n.d.	11	21

*Dense glassy lithic block.
Recalculated anhydrous to 100%; Total, total as analyzed; LOI, loss on ignition at 900°C; $Fe_2O_3 = 0·2$ total Fe as Fe_2O_3; n.d., not determined. Analysts for major elements: J. Taggart, A. Bartel, D. Siems, J. S. Wahlberg, J. Baker, K. Stewart, and D. Vivit. Analyst for trace elements: P. Bruggman.
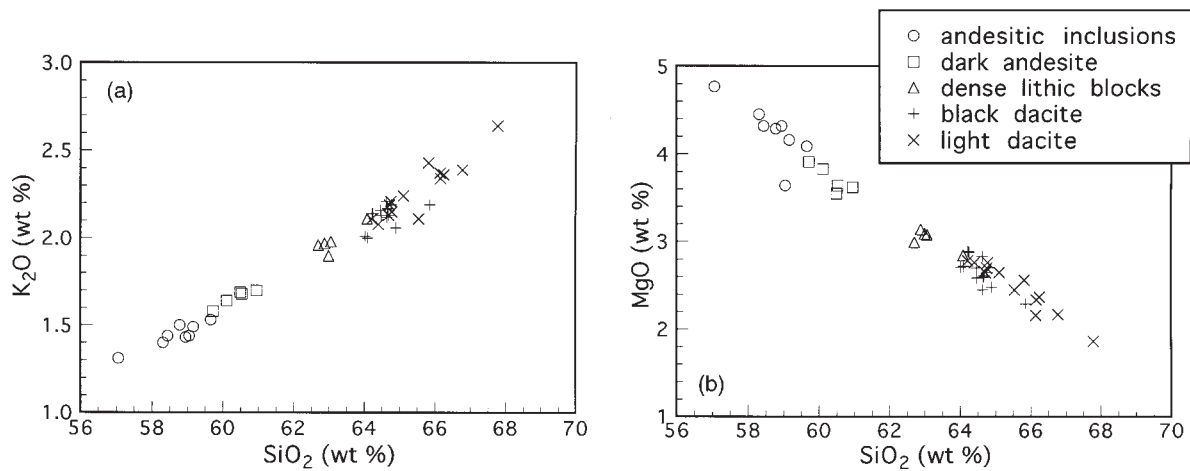
Fig. 5. Variation of (a) K$_2$O and (b) MgO vs SiO$_2$ of the 1915 rocks.

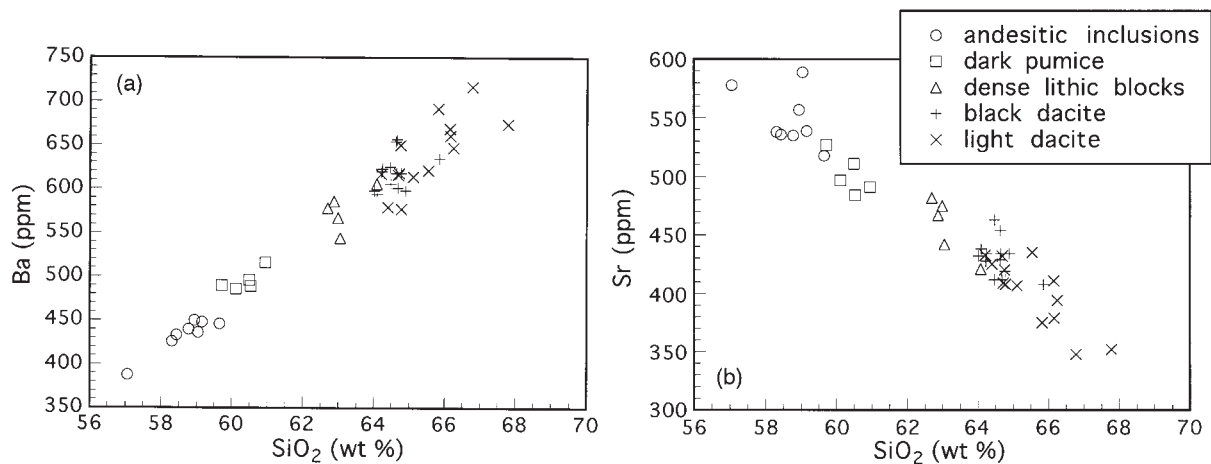**Fig. 6.** Variation of (a) Ba and (b) Sr vs SiO$_2$ of the 1915 rocks.

Silicic end member

The most silicic light dacite samples plot within the range of compositions erupted during the five major silicic eruptions at the Lassen volcanic center in the last 70 ky (Bullen & Clynne, 1990; Clynne, 1990) and also resemble the predominant composition of the next youngest silicic eruption in the Lassen volcanic center, the 1100-year-old dacite of Chaos Crags (Table 9). The unreacted phenocrysts in the light dacite are the same mineral phases and occur in similar relative proportions as for the other young eruptive units at the Lassen volcanic center. For example, large amphibole phenocrysts like those in the 1915 rocks are seen in all the silicic units erupted at the Lassen volcanic center over at least the last 70 ky. Although even the most silicic light dacite shows some evidence of mixing, its composition approaches that of the silicic end member of the 1915 magmas. For the

purpose of mixing calculations presented below, the silicic end member is estimated to have an SiO$_2$ content of ~70 wt %.

Mafic end member

The magma that formed the andesitic inclusions is a logical candidate for the mafic end member of the 1915 rocks. Andesitic inclusions are the most mafic of these rock types and their only phenocryst phase is magnesian olivine. However, the presence of reacted phenocrysts in the andesitic inclusions requires a mixing event in their formation, and the olivine phenocrysts show small amounts of reaction with the groundmass. Reacted phenocrysts are a significant component of the andesitic inclusions (Plate 1d), and they must have been ac-
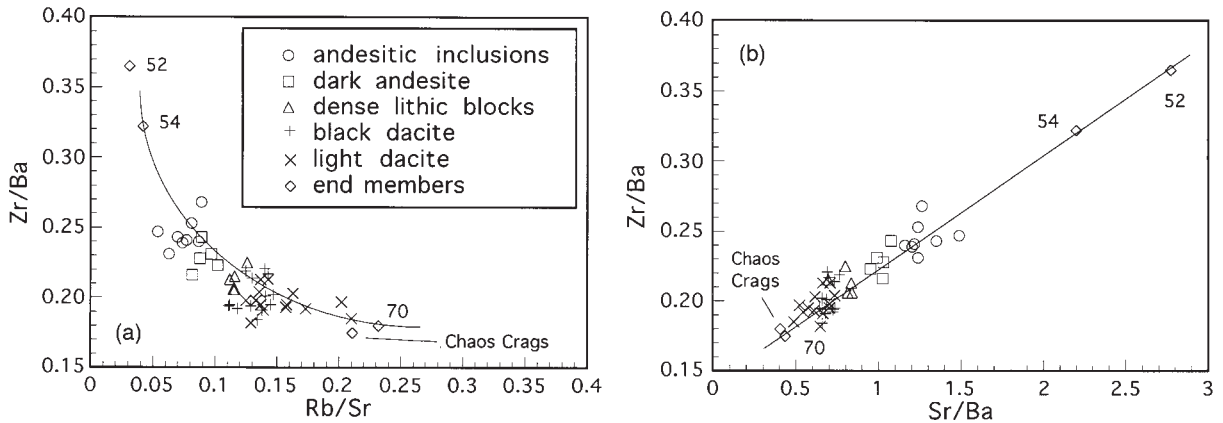
Fig. 7. (a) Zr/Ba vs Rb/Sr diagram for the 1915 rocks and calculated end-member compositions (see text). Compositions of the 1915 rocks plot as a curve, with the calculated end-member compositions fixing the ends of the curve. (b) Zr/Ba vs Sr/Ba companion diagram to (a). The 1915 rocks plot as a straight array in the same relative positions as in (a), indicating a mixing relationship between them.
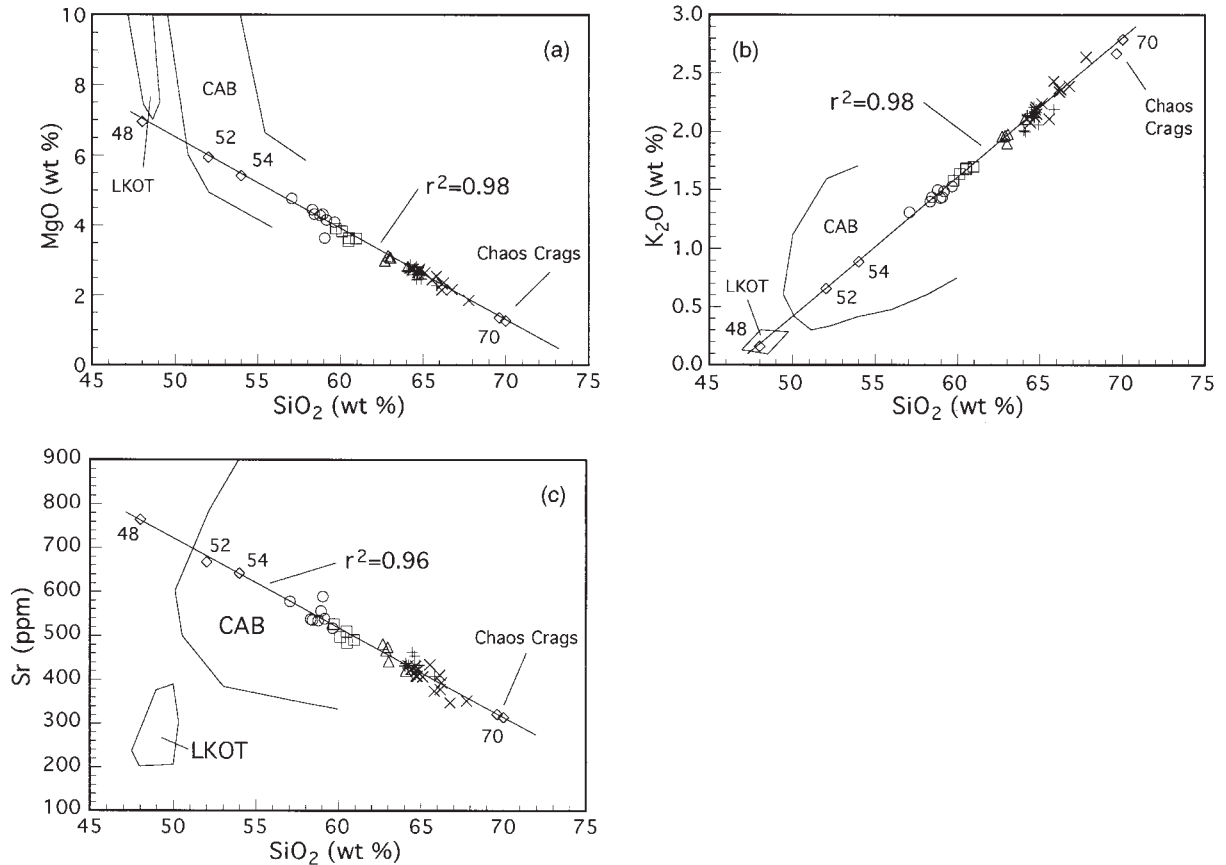
Fig. 8. Plots of the regression of rock analyses for (a) MgO, (b) K_2O, and (c) Sr vs SiO_2. Diamonds labeled 48, 52, 54, 70, and Chaos Crags give the MgO, K_2O, and Sr content of some plausible mixing end members at those SiO_2 contents. Fields labeled LKOT and CAB denote the compositional ranges of mafic magmas in the Lassen area. Legend as in Fig. 7. (See text for further discussion.)

companied by a liquid component now incorporated into the groundmass. Consequently, the andesitic inclusions do not represent the mafic end member of the 1915 magmas.

Table 9: Calculated end-member compositions, and comparison with dacite of Chaos Crags

| | Calculated compositions | | | | | Chaos Crags | |
						Av.*	Inclusion
SiO$_2$	48	52	54	70	69·63	69·63	53·44
Al$_2$O$_3$	20·95	19·91	19·40	15·27	15·36	15·45	18·95
FeOt	8·23	7·20	6·69	2·62	2·71	2·68	7·63
MgO	6·96	5·94	5·42	1·27	1·36	1·33	5·16
CaO	10·83	9·43	8·74	3·18	3·31	3·38	10·33
Na$_2$O	3·49	3·61	3·68	4·23	4·32	4·23	2·75
K$_2$O	0·16	0·66	0·89	2·79	2·67	2·67	0·65
TiO$_2$	0·93	0·82	0·78	0·40	0·41	0·36	0·70
P$_2$O$_5$	0·17	0·16	0·16	0·14	0·14	0·12	0·07
MnO	0·13	0·12	0·11	0·05	0·05	0·06	0·14
Rb (ppm)	9	21	27	73	72	71	12
Sr	765	668	642	314	321	336	582
Ba	121	241	292	778	766	773	179
Zr	76	88	94	140	139	135	70
Ni	89	74	66	5	6	11	23
Cr	123	99	87	0	0	8	36

*Average Chaos Crags computed from 18 analyses of andesitic inclusion-free Chaos Crags dacites, except for Ni and Cr, which are based on two analyses each.

The presence of high-Ni magnesian olivine that contains inclusions of chromian spinel also suggests that the mafic end member was more mafic than any of the 1915 eruptive products. The presence of chromian spinel indicates that the olivine was a near-liquidus phase, and in the Lassen area, only basalts and an uncommon type of basaltic andesite contain this mineralogy (Clynne & Borg, 1997). The composition of the olivine phenocrysts and their high Ni content are appropriate for crystallization from a primitive basalt or basaltic andesite (Luhr & Carmichael, 1985; Clynne & Borg, 1997), but not from a magma with FeO*/MgO = 1·3 and 50 ppm Ni (the bulk composition of the andesitic inclusions).

Two types of primitive olivine basalt and basaltic andesite are present in the Lassen area (Clynne, 1993; Bacon *et al.*, 1997; Borg *et al.*, 1997). Low-K olivine tholeiite (LKOT) typically is aphyric or contains small magnesian olivine phenocrysts and shows remarkably little geochemical variation. LKOT typically contains 48 wt % SiO$_2$, 8–10 wt % MgO, 0·2–0·3 wt % K$_2$O, and is depleted in incompatible elements relative to calc-alkaline basalt. Calc-alkaline basalt and basaltic andesite (CAB) are more diverse in composition. Primitive CAB generally contains phenocrysts of magnesian olivine, may be clinopyroxene-phyric, and typically contains 50–54

wt % SiO$_2$, 6–10 wt % MgO, and 0·3–2·0 wt % K$_2$O. Incompatible-element systematics allow CAB to be divided into incompatible-element-rich and -poor groups (Clynne, 1993; Borg *et al.*, 1997).

Linear regression of the mixing lines and calculation of potential mafic end members at 48, 52, and 54 wt % SiO$_2$ (Table 9) yields compositions that plot within the field of observed CAB for all components, but only for some components of LKOT (Fig. 8a–c). Figure 8c clearly precludes LKOT as an end member for the 1915 rock types. The mineral chemistry observed in the Lassen area basalts further supports this conclusion. The *cr*-number of chromian spinel from LKOT is always <30 (Fig. 3), whereas chromian spinel from CAB has *cr*-numbers that range from 30 to 80 (Clynne & Borg, 1997); The *cr*-number of spinel in 1915 rocks is 49. Furthermore, Ni in Fo$_{84}$ olivine from LKOT is rarely above 1000 ppm, whereas it is generally above 2000 ppm in CAB. In addition, CaO in olivine from LKOT is invariably above 0·25 wt %, but is below that amount in CAB (Clynne & Borg, 1997). The high Ni (2400–2700 ppm) and low CaO (0·11–0·17 wt %) in olivine (Table 4) from the 1915 rocks support a CAB affinity for their mafic end member. Moreover, the high *cr*-number of chromian spinels included in olivine and the low incompatible element contents of both the andesitic inclusions and the calculated mafic end-member magma suggest that the 1915 end member was primitive low-K basaltic andesite (see Clynne & Borg, 1997).

An SiO$_2$ content of 54 wt % (Table 9) for the mafic end member most closely approximates the most mafic and least contaminated undercooled inclusions of the Lassen volcanic center. These occur in the Chaos Crags lavas, are aphyric to sparsely olivine-phyric, and contain 53–54 wt % SiO$_2$ (Table 9). Also, the MgO content of the calculated 54 wt % SiO$_2$ end member would crystallize Fo$_{84}$ olivine at $K_D = 0·3$. Recent experimental work by Baker *et al.* (1994) postulates that primitive low-K basaltic andesites are especially water-rich calcalkaline magmas, and may contain as much as 3–6 wt % water.

MIXING CALCULATIONS

The compositions of mixing end members (Table 9) yield estimates of the proportion of end-member magma in each of the 1915 rock types. Each rock type contains a significant proportion of each end member (Fig. 9). The andesitic inclusions contain 20–35% silicic component, the dark andesite contains 35–45% silicic component, the black dacite contains 30–40% mafic component, and the light dacite contains 15–35% mafic component. About 40–50% of andesitic inclusions must be disaggregated in 70 wt % SiO$_2$ dacite to form the black dacite. This conclusion is supported by the abundance
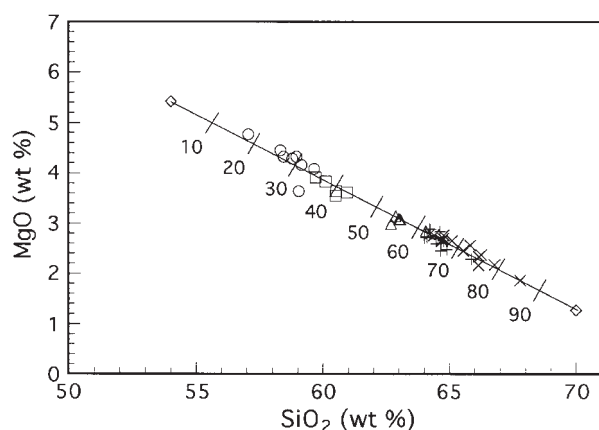
Fig. 9. Mixing line showing proportions of each end member in the rock types plotted on MgO vs SiO$_2$ variation diagram. (See text for rationale behind selection of end-member compositions.) Tick marks on mixing line indicate percent of the silicic end member.

of andesitic inclusion-derived microphenocrysts in the black dacite.

Preliminary volume estimates of the 1915 rocks suggest that subequal amounts of black dacite (2.6×10^6 m^3) and banded pumice [3×10^6 m^3 dense rock equivalent (DRE)] were erupted (Christiansen & Clynne, 1986). The composition of the bulk of the magma erupted resembles that of the black dacite and contains subequal amounts of the mafic and silicic end members. Unless a large proportion of either end member did not erupt, the black dacite approximates the bulk composition of the total system. The ability of a single batch of mafic magma to profoundly affect the composition of a silicic magma body, not only in 1915 but in also in previous magmatic events, argues for a small-volume magma chamber or plexus of small chambers at the Lassen volcanic center (Clynne, 1990).

ORIGIN OF THE 1915 ROCK TYPES
Andesitic inclusions

Undercooled inclusions result from partial quenching of discrete globules of a hotter mafic magma by a cooler silicic one (e.g. Koyaguchi & Blake, 1991). As is clearly the case in the 1915 eruptive products, undercooled inclusions are commonly formed from hybrid magma (Bacon, 1986; Koyaguchi, 1986). The homogeneous distribution and reaction of host-rock phenocrysts in the inclusions, and their lack of crenulate margins suggest that the inclusions were not formed by forcible injection and immediate undercooling into discrete globs. Rather, it is likely that the inclusions are fragments of a layer of hybrid magma.

The following scenario is proposed for formation of the 1915 andesitic inclusions. The mafic end-member magma was injected into the base of a reservoir of silicic magma, and turbulent mixing occurred between them as a fountain of injected magma rose into the host (Campbell & Turner, 1989). Because the resultant hybrid magma is more dense than the host, it fell back to the base of the magma chamber where it accumulated as a layer (Campbell & Turner, 1986; Koyaguchi & Blake, 1991). The range of bulk compositions displayed by the andesitic inclusions (Table 8 and Figs 5, 6, and 9) indicates that the degree of hybridization of the mafic magma during this process did not vary significantly. A stable arrangement of hotter, hybrid magma underneath cooler dacite allows phenocrysts from the dacite component in the hybrid magma to react, even as heat loss to the overlying dacite results in undercooling and rapid crystallization. The observed abundant microphenocrysts, acicular crystal morphologies, and intergrown crystals could all reflect significant degrees of undercooling and convection driven by the strong thermal gradient in the hybrid magma layer (Kouchi et al., 1986).

The hybrid magma vesiculated when a degree of crystallization sufficient to induce vapor saturation of the residual liquid was reached. Eichelberger (1980) called this type of vesiculated layer mafic foam, and demonstrated that it could be less dense than the overlying silicic host. He further proposed that this arrangement would be unstable and that blobs of foam would separate from the hybrid layer and rise into the overlying magma. Eichelberger (1980, fig. 5) proposed a dynamic process wherein blobs of foam were removed from a continually forming layer of relatively constant thickness. Experiments of Turner et al. (1983) showed that vesiculation promotes overturn and mixing in density stratified systems. If 50% crystallization of the hybrid magma had occurred at 1.5–3 kbar pressure, ~3–5 wt % water would cause vesiculation of the lower layer (Huppert et al., 1982). The water-rich mafic end member proposed for the 1915 rocks makes vesiculation a plausible cause of destabilization of the hybrid magma and formation of the andesitic inclusions.

Black dacite

The black dacite contains all three groups of phenocrysts (Table 1). It represents a combination of the silicic end member and disaggregated andesitic inclusions. Three factors could promote the disaggregation of andesitic inclusions, which originally consisted of a network of crystals, vesicles, and ~50% residual liquid. The latter would facilitate plastic deformation and disaggregation during circulation in the magma reservoir (Marsh, 1981; Sparks & Marshall, 1986). Convection induced in the

silicic magma reservoir by heat released from the cooling hybrid layer could allow the vesiculated inclusions to circulate. Mixing might also have been induced by squeezing of the magma batch if it was ascending (Koyaguchi, 1987; Koyaguchi & Blake, 1989).

Light dacite

The light dacite contains all the same petrographic and compositional features as the black dacite and thus the two must have a similar origin. The only significant difference between these rock types is the range of composition seen in light dacite bands and blocks, which is readily attributed to a variable abundance of disaggregated andesitic inclusions. Apparently the magma chamber was zoned, probably in an upward direction. This zonation probably reflected decreased transport of andesitic inclusions and disaggregated crystals to the highest levels in the chamber, but might also have been a relic of preexisting compositional zonation in the silicic end-member magma.

Dark andesite

The close relationship between the dark andesite and the andesitic inclusions is demonstrated by the identical core compositions of their olivine phenocrysts (and included chromian spinels). However, the hopper overgrowths on the olivine phenocrysts from the dark andesite indicate slower cooling and continued crystallization of olivine compared with the (quenched) andesitic inclusions. Two types of reacted phenocrysts are present in dark andesite, one like those in the andesitic inclusions, black dacite, and light dacite, and one that is less reacted and lacks the well-developed overgrowth rims seen in the other rock types. Although compositions of some pyroxene microphenocrysts in the dark andesite resemble those in the andesitic inclusions, these grains are sparse. They are both significantly smaller than and lack the intergrowths observed in the latter. The dark andesite solidified from magma that was of approximately the same composition as that which formed the andesitic inclusions. It was undercooled to the point of nucleation of pyroxene, but not plagioclase, and was quenched upon eruption.

The dark andesite also contains unreacted phenocrysts derived from either the black dacite magma or light dacite magma, reacted phenocrysts with overgrowth rims, and microphenocrysts derived from andesitic inclusions. Hence, although dark andesite lacks large andesitic inclusions, it shows evidence of contamination by both andesitic-inclusion material and crystals derived from the silicic end member. Contamination could occur by: (1) syneruptive mixing between end-member mafic magma

and light dacite magma; (2) syneruptive mixing of an already hybrid dark andesite magma with light dacite magma; or (3) preeruptive homogeneous mixing between end-member or slightly hybridized mafic magma and black dacite magma. The small range of composition of the most mafic dark andesite is difficult to explain by process (1) or (2). Process (3), in which the dark andesite magma originates by homogeneous mixing between the mafic end-member and black dacite magma, avoids the need for a constant minimum amount of syneruptive mixing with light dacite magma. Production of a homogeneous hybrid magma is a logical consequence of downward propagation of the layer of mafic foam.

The downward propagation of mafic foam, followed by formation and disaggregation of andesitic inclusions, has several important consequences for the overlying silicic magma. Heat released by the crystallizing mafic magma would diffuse into the overlying silicic magma and be carried to higher levels by convection. The andesitic inclusions could be transported, either by convection or their own buoyancy, to higher levels in the silicic magma, where their disaggregation would add material to the latter. The result is a decrease in the compositional and thermal difference between the two magmas, which are the two principal factors that control formation of undercooled inclusions (Bacon, 1986). Continued formation and disaggregation of inclusions into the overlying magma reduces the ability of the overlying magma to cool the mafic magma; eventually, formation of mafic foam ceased. Magmas with low thermal and compositional contrast can mix directly (Sparks & Marshall, 1986) to form a homogeneous hybrid. In the 1915 magma chamber, some or all of the remaining mafic magma mixed with black dacite magma to form the magma erupted as the dark andesite.

The formation of andesitic inclusions and dark andesite magma are two extremes of the same mixing process. Early in the mixing history, the temperature and composition contrast between the mafic and silicic magmas was large, and mafic foam formed. Instability of this foam leads to its breakup, and the formation of andesitic inclusions. Eventually, as thermal equilibration greatly reduced the thermal contrast, the addition of a significant portion of mafic magma to the silicic magma by disaggregation of andesitic inclusions reduced the compositional contrast so that the two magmas could mix homogeneously.

Banded pumice

Compositional banding in pumice results from the flow of magma in conduits (Kouchi & Sunagawa, 1985; Koyaguchi, 1985; Blake & Campbell, 1986; Freundt & Tait, 1986). When two liquids of different viscosity are simultaneously drawn into a conduit, the resultant flow is

unstable and the two liquids mix. The textural relationships between the dark andesite and light dacite bands of the 1915 banded pumice suggest that differential flow caused the less viscous magma (dark andesite) to form thin bands that entrain some of the more viscous magma (light dacite), and the more viscous magma to form thicker bands that entrain little of less viscous magma (see Kouchi & Sunagawa, 1985). As magma continues to ascend in the conduit, the bands become thin and the two magmas mix until homogeneity is achieved. The nature of the banding displayed by erupted magma is primarily a function of viscosity contrast, flow velocity, and the length of the conduit. Together, the evidence for a conduit-mixing origin of banded pumice, and theoretical studies of the dynamics of withdrawal of magma from chambers (Blake, 1981a; Blake & Ivey, 1986) explain the textural relationships, relative volumes of dark andesite and light dacite bands in the 1915 banded pumice, and the sequence of eruption products observed in 1915.

THE SEQUENCE OF EVENTS THAT PRODUCED THE 1915 ROCK TYPES

Even though all four of the 1915 rock types are part of the same mixing event between basaltic andesite and dacite, four distinct types of mixing are required to explain them.

Step 1

Basaltic andesite magma intruded the base of the reservoir of dacite magma as a turbulent fountain (Fig. 10a). Mixing in the fountain produced the hybrid andesitic magma, which fell back and accumulated at the base of the chamber. Phenocrysts from the host dacite that were mixed into the mafic magma were reacted. Heat loss to the overlying host dacite caused rapid crystallization and vesiculation of the hybrid magma and produced a layer of mafic foam. Instability and breakup of the foam layer formed the andesitic inclusions (Fig. 10a). Foam was added to the base of the layer by cooling and crystallization, and removed from the top by flotation of andesitic inclusions, so that a more or less constant thickness was maintained. The andesitic inclusions were stirred into the host dacite, both by their own buoyancy and by convection in the dacite magma that was induced by addition of heat from the cooling mafic magma and crystallization of the foam layer (Fig. 10b).

Step 2

Disaggregation of andesitic inclusions into the host dacite magma hybridized the dacite in the main part of the chamber, and produced the black dacite (Fig. 10b).

Step 3

Continued transfer of material and heat from the mafic magma to the silicic magma by foaming and convection caused the temperature of the black dacite magma to rise and its viscosity to decrease. Eventually, the black dacite magma could no longer cool the mafic magma to the point of vesiculation (Fig. 10c). Mixing then occurred directly across the interface of the two magmas, and a new layer of hybrid magma, the dark andesite magma, was formed. This may have triggered the 1915 eruption.

At the end of this step, the magma chamber consisted of three magma types—dark andesite magma, overlain by black dacite magma zoned upward to the light dacite magma. The rise in temperature and volatile pressure, and concomitant decrease in viscosity and density of the black dacite magma caused it to rise through the light dacite magma. This provoked fracturing of the wallrock, and initiated propagation of a conduit to the surface (Sparks et al., 1977; Blake, 1981b; Huppert et al., 1982). Black dacite magma began to empty from the chamber into the conduit and rose toward the surface. Heating of groundwater in the volcano and degassing of the conduit magma caused the phreatic activity from May 1914 to May 1915. Meanwhile, the rise in temperature of the black dacite and light dacite magmas, disaggregation of volatile-rich inclusions, and perhaps dehydration of hydrous minerals (Bardintzeff & Bonin, 1987; Mazzone et al., 1987) increased the volatile pressure in the magma chamber. From May 14 to May 19, 1915, the magma in the conduit was squeezed out into the crater, building the lava dome at the summit of Lassen Peak (Fig. 10c). On the evening of May 19, new, less degassed black dacite reached the vent, and caused the explosion that destroyed the lava dome and initiated the avalanche. Black dacite then erupted from the vent and formed the two lava flow lobes.

Step 4

Enough of the black dacite magma erupted so that the magma withdrawal front intersected the interface between black dacite magma and dark andesite magma. Simultaneous tapping of the two magmas and mixing in the conduit during ascent produced the banded pumice erupted on May 22 (Fig. 10d). Magma dragged into the conduit from near the top of the chamber erupted as light dacite pumice on May 22, 1915.

CONCLUSIONS

(1) All four rock types in the 1915 eruption sequence of Lassen Peak show evidence of magma mixing.
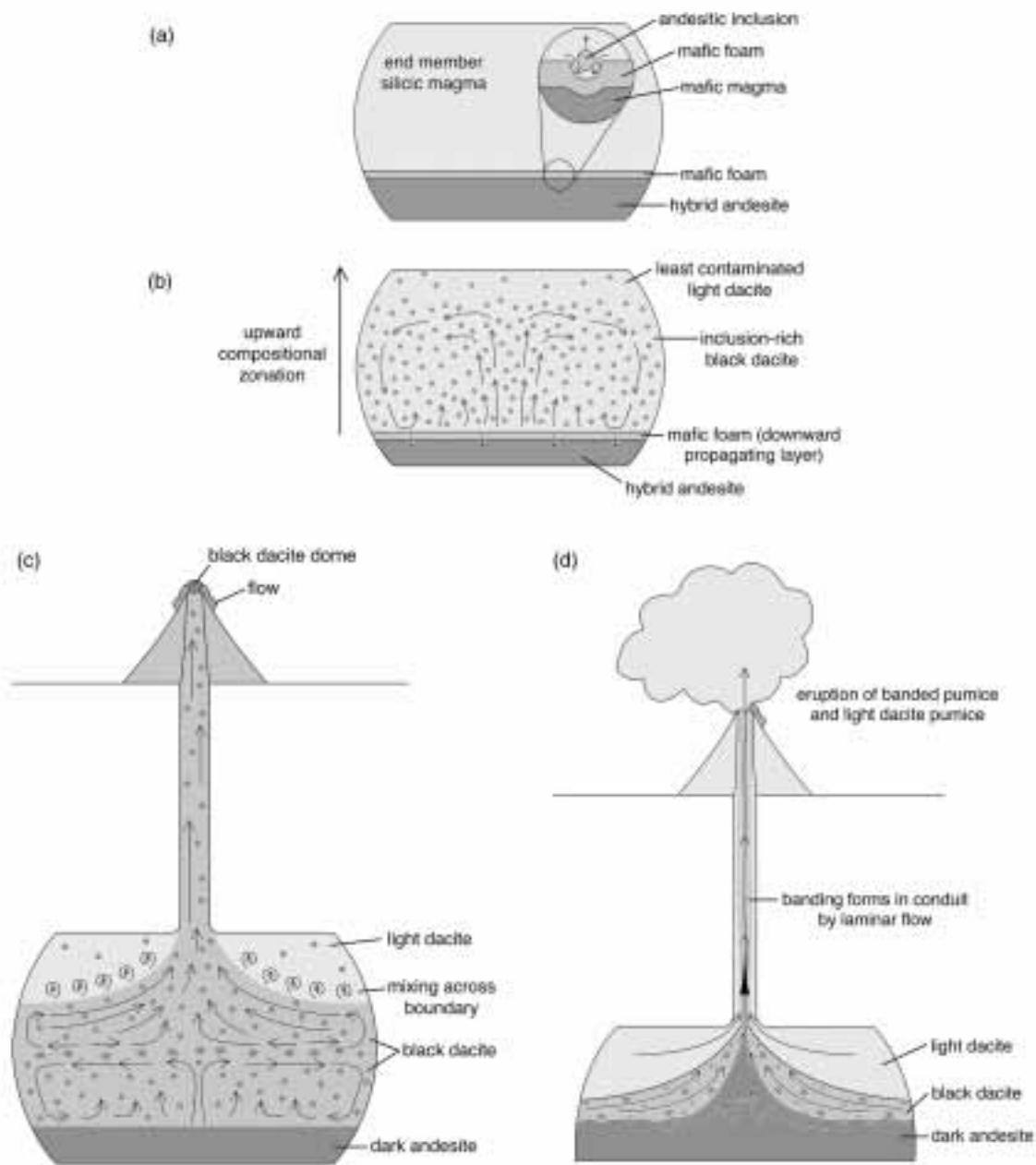
Fig. 10. Schematic depiction of the 1915 magma chamber and formation of the 1915 rocks: (a) mafic foam and andesitic inclusions; (b) black dacite magma; (c) magma chamber during eruption of the black dacite, May 14–19; (d) magma chamber during eruption of the banded pumice and light dacite, May 22. The size and shape of the magma chamber depicted is for the convenience of the presentation. The actual configuration may have been much different.

(2) The most silicic light dacite (68 wt % SiO_2) approaches the composition of the silicic end member (69–70 wt % SiO_2), but the composition of the probable mafic end member (54 wt % SiO_2) is somewhat more mafic than the most mafic eruption product, the andesitic inclusions (57–60 wt % SiO_2).

(3) Homogeneous mixing of magmas produced the andesitic inclusion magma and the dark andesite magma. Back mixing by disaggregation of the andesitic inclusions into light dacite magma formed the black dacite magma. Heterogeneous or incomplete mixing formed the banded pumice.

(4) Disaggregation of andesitic inclusions played an important role in forming the intermediate magmas that erupted in 1915.

(5) Cycling of phenocrysts through partially crystallized undercooled inclusions explains the coexistence of strongly reacted and unreacted phenocryst populations. This process explains the generation of disequilibrium phenocryst assemblages and features in many volcanic rocks of intermediate composition.

ACKNOWLEDGEMENTS

REFERENCES

Albee, A. L. & Ray, L. (1970). Correction factors for electron micro-analysis of silicates, oxides, carbonates, phosphates, and sulfates. *Analytical Chemistry* **42,** 1408–1414.

Bacon, C. R. (1986). Magmatic inclusions in intermediate and silicic volcanic rocks. *Journal of Geophysical Research* **91,** 6091–6112.

Bacon, C. R. & Druitt, T. H. (1988). Compositional evolution of the zoned calc-alkaline magma chamber of Mount Mazama, Crater Lake, Oregon. *Contributions to Mineralogy and Petrology* **98,** 224–256.

Bacon, C. R., Bruggman, P. E., Christiansen, R. L., Clynne, M. A., Donnelly-Nolan, J. L. & Hildreth, W. (1997). Primitive magmas at five Cascades volcanic fields: melts from hot, heterogeneous sub-arc mantle. *Canadian Mineralogist* **35,** 397–423.

Baker, M. B., Grove, T. L. & Price, R. (1994). Primitive basalts and andesites from the Mt. Shasta region, N. California: products of varying melt fraction and water content. *Contributions to Mineralogy and Petrology* **118,** 111–129.

Bardintzeff, J.-M. & Bonin, B. (1987). The amphibole effect: a possible mechanism for triggering explosive eruptions. *Journal of Volcanology and Geothermal Research* **33,** 255–262.

Bence, A. E. & Albee, A. L. (1968). Empirical correction factors for the electron microanalysis of silicates and oxides. *Journal of Geology* **76,** 382–403.

Blake, S. (1981a). Eruptions from zoned magma chambers. *Journal of the Geological Society, London* **138,** 281–287.

Blake, S. (1981b). Volcanism and the dynamics of open magma chambers. *Nature* **289,** 783–785.

Blake, S. & Campbell, I. H. (1986). The dynamics of magma-mixing during flow in volcanic conduits. *Contributions to Mineralogy and Petrology* **94,** 72–81.

Blake, S. & Ivey, G. N. (1986). Magma-mixing and the dynamics of withdrawal from stratified reservoirs. *Journal of Volcanology and Geothermal Research* **27,** 153–178.

Borg, L. E., Clynne, M. A. & Bullen, T. D. (1997). The variable role of slab-derived fluids in the generation of a suite of primitive calc-alkaline lavas from the southernmost Cascades, California. *Canadian Mineralogist* **35,** 425–452.

Bullen, T. D. & Clynne, M. A. (1990). Trace element and isotopic constraints on magmatic evolution at Lassen volcanic center. *Journal of Geophysical Research* **95,** 19671–19691.

Campbell, I. H. & Turner, J. S. (1986). Fountains in magma chambers. *Journal of Petrology* **27,** 1–30.

Campbell, I. H. & Turner, J. S. (1989). The influence of viscosity on fountains in magma chambers. *Journal of Petrology* **30,** 885–923.

Cashman, K. V. & Bergantz, G. W. (1991). Magmatic processes. *Reviews of Geophysics, Supplement, US National Report to International Union of Geodesy and Geophysics* **1987–1990,** 500–512.

Christiansen, R. L. & Clynne, M. A. (1986). The climactic eruptions of Lassen Peak, California, in May, 1915 (abstract). *Eos Transactions, American Geophysical Union* **67,** 1247.

Clynne, M. A. (1989). Disaggregation of quenched magmatic inclusions contributes to chemical heterogeneity in silicic lavas of Lassen Peak, California. *New Mexico Bureau of Mines and Mineral Resources, Bulletin* **131,** 54.

Clynne, M. A. (1990). Stratigraphic, lithologic, and major element geochemical constraints on magmatic evolution at Lassen volcanic center, California. *Journal of Geophysical Research* **95,** 19651–19669.

Clynne, M. A. (1993). Geologic studies of the Lassen volcanic center, Cascade Range, California. Ph.D. Thesis, University of California, Santa Cruz.

Clynne, M. A. & Borg, L. E. (1997). The composition of olivine and chromian spinel in primitive calc-alkaline and tholeiitic lavas from the southernmost Cascade Range, California: a reflection of relative fertility of the source. *Canadian Mineralogist* **35,** 453–472.

Clynne, M. A. & Christiansen, R. L. (1987). Magma mixing and the devastating eruptions of May 1915 at Lassen Peak, California (abstract). *Hawaiian Volcano Observatory Symposium on How Volcanoes Work, Hilo, Hawaii, January 1987, Abstract Volume*, p. 43.

Coulon, C., Clocchiatti, R., Maury, R. C. & Westercamp, D. (1986). Petrology of basaltic xenoliths in andesitic to dacitic host lavas from Martinique (Lesser Antilles): evidence for magma mixing. *Bulletin Volcanologique* **47,** 705–734.

Eichelberger, J. C. (1980). Vesiculation of mafic magma during replenishment of silicic magma reservoirs. *Nature* **288,** 446–450.

Feeley, T. C. & Dungan, M. A. (1996). Compositional and dynamic controls on mafic–silicic magma interactions at continental arc volcanoes: evidence from Cordon El Guadal, Tatara–San Pablo Complex, Chile. *Journal of Petrology* **37,** 1547–1577.

Freundt, A. & Tait, S. (1986). The entrainment of high-viscosity magma into low-viscosity magma in eruption conduits. *Bulletin of Volcanology* **48,** 325–339.

Gill, J. B. (1981). *Orogenic Andesites and Plate Tectonics*. New York: Springer-Verlag.

Heiken, G. & Eichelberger, J. C. (1980). Eruptions at Chaos Crags, Lassen Volcanic National Park, California. *Journal of Volcanology and Geothermal Research* **7,** 443–481.

Huppert, H. E., Sparks, R. S. J. & Turner, J. S. (1982). Effects of volatiles on mixing in calc-alkaline magma systems. *Nature* **297,** 554–557.

Kouchi, A. & Sunagawa, I. (1985). A model for mixing basaltic and dacitic magmas as deduced from experimental data. *Contributions to Mineralogy and Petrology* **89,** 17–23.

Kouchi, A., Tsuchiyama, A. & Sunagawa, I. (1986). Effect of stirring on crystallization kinetics of basalt: texture and element partitioning. *Contributions to Mineralogy and Petrology* **93,** 429–438.

Koyaguchi, T. (1985). Magma mixing in a conduit. *Journal of Volcanology and Geothermal Research* **25,** 365–369.

Koyaguchi, T. (1986). Evidence for two-stage mixing in magmatic inclusions and rhyolitic lava domes on Niijima Island, Japan. *Journal of Volcanology and Geothermal Research* **29,** 71–98.

Koyaguchi, T. (1987). Magma mixing in a squeezed conduit. *Earth and Planetary Science Letters* **84,** 339–344.

Koyaguchi, T. & Blake, S. (1989). The dynamics of magma mixing in a rising batch. *Bulletin of Volcanology* **52,** 127–137.

Koyaguchi, T. & Blake, S. (1991). Origin of mafic enclaves: constraints on the magma mixing model from fluid dynamic experiments. In: Didier, J. & Barbarin, B. (eds) *Enclaves and Granite Petrology. Developments in Petrology, Vol. 13*. Amsterdam: Elsevier, pp. 415–429.

Leake, B. E. (1978). Nomenclature of amphiboles. *Canadian Mineralogist* **16,** 511–520.

Lindsley, D. H. & Anderson, D. J. (1983). A two-pyroxene thermometer. *Proceedings of the 13th Lunar and Planetary Science Conference, Part 2. Journal of Geophysical Research* **88,** A887–A906.

Linneman, S. R. & Myers, J. D. (1990). Magmatic inclusions in the Holocene rhyolites of Newberry Volcano, central Oregon. *Journal of Geophysical Research* **95,** 17677–17691.

Lofgren, G. E. (1980). Experimental studies on the dynamic crystallization of silicate melts. In: Hargraves, R. B. (ed.) *Physics of Magmatic Processes*. Princeton, NJ: Princeton University Press, pp. 487–551.

Luhr, J. F. & Carmichael, I. S. E. (1985). Jorullo volcano, Michoacan, Mexico (1759–1774): the earliest stages of fractionation in calc-alkaline magmas. *Contributions to Mineralogy and Petrology* **90,** 142–161.

Macdonald, G. A. & Katsura, T. (1965). Eruption of Lassen Peak, Cascade Range, California, in 1915: example of mixed magmas. *Geological Society of America Bulletin* **76,** 475–482.

Marsh, B. D. (1981). On the crystallinity, probability of occurrence, and rheology of lava and magma. *Contributions to Mineralogy and Petrology* **78,** 85–98.

Mazzone, P., Stewart, D. C. & Hughes, J. H. (1987). Sub-solidus dehydration of amphiboles in an andesitic magma. *Contributions to Mineralogy and Petrology* **97,** 292–296.

Morimoto, N., Fabries, J., Ferguson, A. K., Ginzburg, I. V., Ross, M., Seifert, F. A., Zussman, J., Aoki, K. & Gottardi, G. (1988). Nomenclature of pyroxenes. *American Mineralogist* **73,** 1123–1133.

Papike, J. J., Cameron, K. L. & Baldwin, K. (1974). Amphiboles and pyroxenes: characterization of other than quadrilateral components and estimates of ferric iron from microprobe data (abstract). *Geological Society of America, Abstracts with Programs* **6,** 1053–1054.

Philpotts, A. R. (1990). *Principles of Igneous and Metamorphic Petrology*. Englewood Cliffs, NJ: Prentice–Hall.

Rutherford, M. J. & Hill, P. M. (1993). Magma ascent rates from amphibole breakdown: an experimental study applied to the 1980–1986 Mount St. Helens eruptions. *Journal of Geophysical Research* **98,** 19667–19685.

Sakuyama, M. (1984). Magma mixing and the magma plumbing systems in island arcs. *Bulletin Volcanologique* **47,** 685–703.

Sparks, R. S. J. & Marshall, L. A. (1986). Thermal and mechanical constraints on mixing between mafic and silicic magmas. *Journal of Volcanology and Geothermal Research* **29,** 99–124.

Sparks, R. S. J., Sigurdsson, H. & Wilson, L. (1977). Magma mixing: a mechanism for triggering acid explosive eruptions. *Nature* **267,** 315–318.

Taggart, J. E., Jr, Lindsey, J. R., Scott, B. A., Vivit, D. V., Bartel, A. J. & Stewart, K. C. (1987). Analysis of geologic materials by wavelength-dispersive X-ray fluorescence spectrometry. *US Geological Survey Bulletin* **1170,** E1–E19.

Thompson, R. A. & Dungan, M. A. (1985). The petrology and geochemistry of the Handkerchief Mesa mixed magma complex, San Juan Mountains, Colorado. *Journal of Volcanology and Geothermal Research* **26,** 251–274.

Tsuchiyama, A. (1985). Dissolution kinetics of plagioclase in the melt of the system diopside–albite–anorthite, and the origin of dusty plagioclase in andesites. *Contributions to Mineralogy and Petrology* **89,** 1–16.

Turner, J. S. & Campbell, I. H. (1986). Convection and mixing in magma chambers. *Earth-Science Reviews* **23,** 255–352.

Turner, J. S., Huppert, H. E. & Sparks, R. S. J. (1983). An experimental investigation of volatile exsolution in evolving magma chambers. *Journal of Volcanology and Geothermal Research* **16,** 263–277.

Turrin, B. D., Christiansen, R. L., Clynne, M. A., Champion, D. E., Gerstel, W. J., Muffler, L. J. P. & Trimble, D. A. (1998). The age of Lassen Peak, California, and implications for the ages of latest Pleistocene glaciations in the southern Cascade Range. *Geological Society of America, Bulletin* **110,** 931–945.

Ussler, W., III (1988). Experimental and theoretical studies of mixed magmas. Ph.D. Dissertation, University of North Carolina at Chapel Hill.

Williams, H. (1932). Geology of the Lassen Volcanic National Park, California. *University of California, Department of Geological Sciences Bulletin* **21,** 195–385.